JPhys Materials

TOPICAL REVIEW • OPEN ACCESS

Towards low- loss on-chip nanophotonics with coupled graphene and silicon carbide: a review

To cite this article: Patrick Rufangura et al 2020 J. Phys. Mater. 3 032005

View the article online for updates and enhancements.

Recent citations

- <u>The topological criticality in disordered</u> non-Hermitian system Xi-Xi Bao *et al*
- Ultrabroad-Band Direct Digital Refractive Index Imaging Based on Suspended Graphene Plasmon Nanocavities Xiaofei Xiao et al
- Energy Plasmon Modes in Metamaterialfilled Double-layer Graphene-wrapped Cylindrical Waveguides M. Saeed *et al*

Journal of Physics: Materials



OPEN ACCESS

RECEIVED

29 February 2020

REVISED

5 June 2020

ACCEPTED FOR PUBLICATION 15 June 2020

PURUSHED

14 July 2020

Original content from this work may be used under the terms of the Creative Commons Attribution 4.0 licence.

Any further distribution of this work must maintain attribution to the author(s) and the title of the work, journal citation and DOI.



Topical Review

Towards low- loss on-chip nanophotonics with coupled graphene and silicon carbide: a review

Patrick Rufangura 10, Thomas G Folland 2,3, Arti Agrawal 4, Joshua D Caldwell and Francesca Iacopi 4,40

- School of Electrical and Data Engineering, Faculty of Engineering and IT, University of Technology Sydney, Broadway, 2007 NSW, Australia
- ² Department of Mechanical Engineering, Vanderbilt University, Nashville, TN 37212, United States of America
- Department of Physics and Astronomy, The University of Iowa, Iowa City IA, 52242, United States of America
- ⁴ Australian Research Council Centre of Excellence on Transformative Meta-Optical Systems, University of Technology Sydney, Broadway, 2007 NSW, Australia

E-mail: francesca.iacopi@uts.edu.au

Keywords: graphene, silicon carbide, surface plasmon polariton, surface phonon polariton, electromagnetic hybrid modes, metamaterials

Abstract

The ability to control the interaction of light and matter at the nanoscale is at the heart of the field of nanophotonics. This subdiffractional confinement of light can be achieved through the stimulation of surface polaritons, most notably surface plasmon polaritons (SPPs). However, the high optical losses and lack of tunability of conventional plasmonic materials have hindered major progress in this field. In the search for alternative low-loss and tunable materials, graphene and polar dielectric materials are viewed as potential alternatives to more common metal-based plasmonic materials. In particular, the possibility of combining the tunable nature of graphene SPPs with the high-quality factors and long lifetimes of surface phonon-polaritons (SPhPs) modes supported in polar dielectric materials (e.g. SiC) offers great promise for advanced nanophotonic applications. The combination of graphene SPPs and SPhPs supported in SiC is even more pertinent as this material system can be realized in the form of epitaxial graphene (EG), whereby sublimation of silicon from a SiC results in a surface reconstruction into a graphene surface termination. This offers an ideal technology platform for realizing hybrid SPP-SPhP modes. In this review, we outline advances in graphene plasmonics and the generation of SPhPs in polar materials, in the context of epitaxial graphene. We review recent attempts at realizing such coupling of graphene SPPs with phonon and SPhP modes in SiC, as well as covering such modes in other polar materials and conclude with an overview of advantages and challenges for further advancement of nanophotonics based on graphene on silicon carbide for on-chip light manipulation.

1. Introduction

Graphene is a highly promising material for a variety of applications in the photonics industry due to its exceptional optical, physical, electrical, and mechanical properties [1, 2]. One of the most anticipated impacts is found in the potential for miniaturization of devices, where graphene can be transferred to microor nano-scale devices to enhance their performance or add additional functionality [3, 4]. While the transfer of graphene onto different substrates and pre-fabricated structures is possible [5, 6], another appealing route is the direct growth of graphene on a given material [7–9]. A breakthrough was achieved with the epitaxial growth of graphene on silicon carbide, which emerged as an alternative to avoid transfer-based methods [3]. The ability to grow graphene directly on a semiconductor substrate enables graphene-based optical, optoelectronic, and electronic devices at scale.

One of the exciting aspects of exploring graphene and silicon carbide is their ability to support surface plasmon polaritons (SPPs) and surface phonon polaritons (SPhPs), respectively. Polaritons provide deep sub-wavelength confinement of light and have enabled many photonic applications such as passive radiative

cooling [10, 11], cancer detection and therapies [12, 13], assessment of energy efficiency of buildings [14], biological and chemical sensing [15–18], among others [19–28]. Graphene and silicon carbide have also been extensively studied separately in the literature as potential photonic materials [27, 29–35]. While the expanding fields of graphene SPPs and SPhPs are too extensive for a complete analysis within a single review, instead these have been the subject of their own direct reviews [23, 27, 29, 36]. As such, in this review, we focus on aspects related to the hybrid system of graphene on silicon carbide, specifically in regards to epitaxial graphene (EG), highlighting its promise for mid-infrared (MIR) nanophotonic applications featuring low-loss and extreme sub-diffractional confinement. We will highlight how this platform provides unique potential due to the relative ease of fabrication, as well as the favourable properties of both graphene and silicon carbide for a variety of infrared (IR) nanophotonics concepts.

1.1. The diffraction limit—a challenge for miniaturization

Conventional optics make use of materials with a positive real part of the dielectric function to propagate and manipulate electromagnetic (EM) waves at optical frequencies. The benefits associated with the use of plane waves and refractive optics is that they enable propagation and manipulation of light over long distances with comparative ease. However, as a consequence of the diffraction limit first reported by Ernst Abbe in 1873, a beam of light traveling in a medium with refractive index and a converging half-angle θ , a minimum resolvable size of $d = \frac{\lambda}{2NA}$ results, where NA is the numerical aperture of the lens and NA = $nsin\theta$. For a microscope objective of NA = 1, the minimum focal spot is $d = \frac{\lambda}{2}$, from roughly a quarter of a micron for the blue end of the visible spectrum and extending to several microns for longer-wavelength infrared light [27, 37, 38]. As such, for mid-wave to long-wave IR light, the focusing of light to nanoscale dimensions is not realistic. As such wavelengths of light are advantageous for many applications ranging from vibrational spectroscopy enabling insights into the composition of chemicals and materials, provide a non-contact monitor of temperature, offers the promise of minimal free-space attenuation of light by the atmosphere, as well as limiting light-induced damage on samples of interest associated with higher frequency light sources. However, the long-wavelengths that enable these applications also imply that the requisite optical components must also be wavelength scale or larger, limiting opportunities for compact solutions. Thus, there are a strong desire for photonic solutions that enable operations beyond the diffraction limit, which has sparked a substantial body of literature over recent years in polaritonics, and metamaterials [39].

1.2. Sub-diffractional confinement with plasmonics

While there are a number of reviews discussing the basics of plasmonics [38, 40–44], a brief overview is provided here for clarity. In contrast to traditional refractive optical materials, metallic materials have a negative real part of the dielectric function, whereby free carriers oscillate coherently in response to incident optical fields, screening out the radiation and resulting in high reflectivity. It is within spectral regions where the real part of the permittivity is negative that a material can support SPPs, and thus provide the means to develop sub-diffractional photonics [44, 45]. This behaviour can be modelled via the Drude function, which beyond metals is also readily employed in the infrared to describe the optical response of highly doped semiconductors, via the dispersion relation:

$$\varepsilon(\omega) = \varepsilon_{\infty} - \frac{\omega_{\rm p}^2}{\omega^2 + i\gamma\omega} \tag{1}$$

where ω is the angular frequency, while ω_p , and γ are the plasma frequency and damping constant associated with the free-carrier plasma oscillation in the metal, respectively. The plasma frequency designates the highest frequency at which the free carriers in a given material can coherently respond to an incident electromagnetic field, defined as:

$$\omega_p = \sqrt{\frac{ne^2}{m^* \varepsilon_0}} \tag{2}$$

with n,m^* e, and ε_0 representing the free carrier density, the effective mass of the charge carrier, elementary charge, and the permittivity of vacuum, respectively. We also define $\tau = \frac{1}{\Gamma}$ as the relaxation time of free electrons. From (2) the dc- conductivity (σ_0) of the material can be estimated in terms of plasma frequency [40].

$$\sigma_0 = \frac{ne^2\tau}{m} = \omega_p \tau \varepsilon_0 \tag{3}$$

The plasma frequency also defines the upper-frequency limit where SPPs can be stimulated in the material. A SPP is a hybrid mode comprised of light coupled to a coherent oscillation of free-charge carriers. In planar slabs, excitation of SPPs results in a propagating mode confined to the interface between the

polaritonic medium and the surrounding dielectric (e.g. air), which offers the opportunity to compress the electromagnetic energy to deeply subwavelength scales [46–49]. SPPs can also be realized in highly confined geometries through the formation of deeply subdiffractional cavities and nanostructures. SPPs have enabled several applications, such as biosensors [50], enhanced photovoltaic cells [51, 52], photothermal-therapies [13, 53, 54], optical interconnects [55], and metamaterial-based concepts and devices [56–62]. However, for most applications, the optical losses must be low. Thus, the imaginary part of the dielectric permittivity must be small, specifically much smaller than the absolute value of the real part. In this respect, metals such as Au, Ag, Al, and Cu are considered as the best plasmonic materials in the visible spectrum [47, 63, 64]. Yet, the plasma frequency of metals in the visible range results in much larger (<-1000) real dielectric permittivities than the adjacent dielectric (~1–10) in the MIR, hence a thin metal film produces weak confinement of light in the MIR range. Moreover, the carrier density of metals cannot be dynamically tuned. Metal-based SPP modes can only be tuned with the use of alloys (this also reduces the mobility and increases impurity scattering) or by adjusting their geometrical parameters in the design stage [65]. Studies focused on identifying alternative plasmonic materials with low optical losses have been conducted on heavily doped semiconductors and conductive oxides [37, 65–69]. However, one of the challenges with the semiconductors is that excess doping in semiconductors typically degrades mobility and thus increases the losses [65], with the notable exception of materials such as n-type CdO, where the carrier mobility (imaginary part of the dielectric function) is found to increase (decrease) as the doping density is increased, even up to levels as high as 3×10^{20} cm⁻³ [70–72]. However, such a material is the exception, and thus, in most cases, there is a fundamental trade-off between controlling the plasma frequency for spectral tuning, and realizing sufficiently low losses for a given application. This has motivated research to expand into a broader range of polaritonic materials, such as 2D and polar materials [42, 73, 74].

2. Dispersion relation of SPP modes

Much of the physics of polaritonic modes can be understood by exploring the dispersion of plasmonic materials [75–77]. Considering a planar interface between a non-dispersive dielectric material featuring a positive permittivity ε_d and a conducting material (e.g. doped semiconductor) with a complex dielectric function $\varepsilon_m(\omega)$, exhibiting a negative real part, a deeply subwavelength evanescent SPP mode can be established at this interface (see figure 1(a)) with wave vector k_x .

The dispersion of the SPP (k_{SPP}) mode can be obtained from the solution to Maxwell's equation for the two-layer system discussed above, once sufficient boundary conditions are applied [40, 78], with the in-plane wavevector defined as:

$$k_{x} = k_{0} \sqrt{\frac{\varepsilon_{d} \varepsilon_{m}(\omega)}{(\varepsilon_{m}(\omega) + \varepsilon_{d})}}$$

$$\tag{4}$$

where $k_0 = \frac{\omega}{c}$ represents the wavevector in free space. Using the complex dielectric function of doped InAs [63] within equation (4), we can calculate the dispersion of the SPP mode at the surface of a doped InAs slab and air (figure 1(c)). The dispersion curve indicates that at low frequencies, the SPP mode lies near the dispersion of light in free space (red, so-called 'light-line,' figure 1(c)), indicating that the SPP has a wavelength similar to that of light propagating in air. However, as the frequency is increased, the dispersion curve and light-line separate, with the k_{SPP} becoming significantly larger than free-space light $k_{SPP} > k_0$, asymptotically approaching the SPP resonant frequency ($\omega_{spp} = \frac{\omega_p}{\sqrt{\varepsilon_d + 1}}$) [78]. Here ω_{spp} stands for the frequency of SPP resonance. At this frequency, the wavevector converges to its largest value ($k_{SPP} \to \infty$), thus the corresponding SPP wavelength (λ_{SPP}) becomes vanishingly small ($\lambda_{SPP} \to 0$). It is this exceptional wavelength reduction that enables the desired strong confinement of optical fields to subdiffractional dimensions [63, 78]. However, this also imposes a large momentum mismatch with free space light that must be overcome for the excitation of SPP modes.

There are several ways to manipulate incident light to match that of an SPP mode [38]. One method is to shrink the wavelength of light through a high index prism [79–81], which is placed on (Kretschmann configuration), or in close proximity (Otto configuration) to the polaritonic surface. When the angle of the incident (θ_i) light in the prism and the adjacent material is greater than a critical angle (θ_c), total internal reflection occurs, which results in an evanescent mode that can launch an SPP of the same wavevector and frequency. Alternatively, the launching of SPPs can be realized through a grating, whereby the reduced momentum of diffractive modes dictated by the periodicity of the grating [82] can be used to slow down the incident light for this purpose. Finally, Mie-scattering from sub-wavelength polaritonic nanoparticles defines a fixed wavevector for the polariton mode dictated by the size of the structure, resulting in a defined resonant frequency [83–85]. Further details concerning the dispersion of SPP modes and coupling techniques were discussed in these references [38, 40, 75, 78, 86].

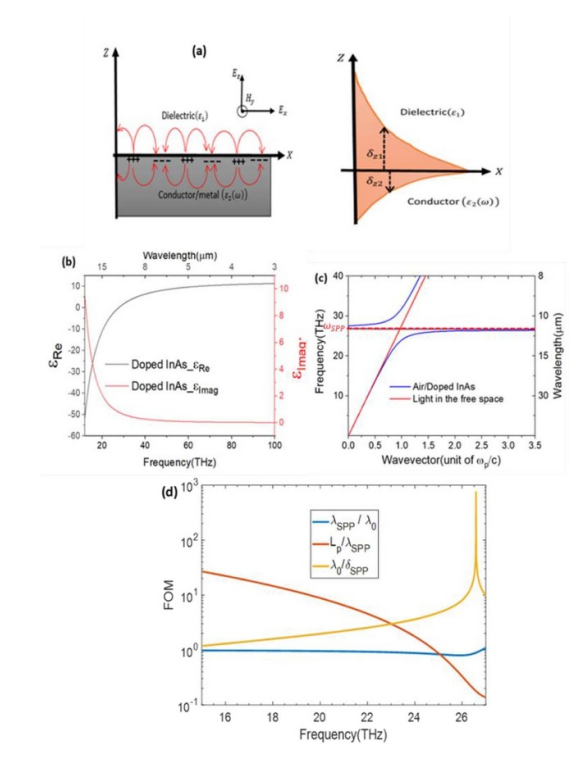


Figure 1. (a) Schematics illustrating the SPP mode at the flat interface between air and a conductor (left), and the penetration depth (how the field intensities decay) in dielectric and conductor (right), (b) The calculated permittivity (real and imaginary) of doped InAs using the Drude model (1). (c) The calculated dispersion relation of the air and doped InAs's interface compared with the dispersion of light in the free space (solid red line). The horizontal broken line denotes the position of surface plasmon resonance frequency ($\omega_{spp} \cong 27.7 \ THz$). (d) The calculated figures of merit for three-length scales characteristics of SPP mode in doped InAs. The calculations were performed using the data for doped InAs ($\varepsilon_{\infty} = 12.3$, $\omega_p = 1.74 \times 10^{14} \frac{rad}{s}$, and relaxation time $t = 8.85 \times 10^{-14} s$) from [67].

There are also three-length scales that play a crucial role in the characterization of SPP modes. The first is λ_{SPP} , which defines the period of the oscillating surface charge density and the subdiffractional field extent and distribution. The λ_{SPP} can be obtained from the real part of the SPP wave vector (\mathbf{k}_{SPP}') , $(\lambda_{SPP} = \frac{2\pi}{\mathbf{k}_{SPP}'})$. The second is the length-scale of the SPP propagation (L_p) and refers to a distance over which the evanescent field will decay to 1/e from the maximum intensity along the direction of propagation and is related to the imaginary wavevector (k''_{SPP}) , $(L_p = \frac{1}{2k''_{SPP}})$. Usually, the propagation length of the SPP mode will vary from a few hundred nms to hundreds of microns depending on the loss and the magnitude of the negative real part of the dielectric function of the polaritonic medium. For localized resonant structures, the performance metric is typically designated via the quality factor, defined as $\omega_{res}/\Delta\omega$, where ω_{res} and $\Delta\omega$ represents the resonant frequency and linewidth of the SPP resonance. The Q-factor defines the number of field oscillations that the SPP mode will undergo within the cavity before dissipation [27]. The third is the evanescent extent of the polaritonic fields (in plasmonic material and dielectric), which denotes the distance over which the intensity of field decays 1/e of the maximum intensity in the direction perpendicular to the propagation direction $(\delta_{SPP} = \frac{1}{Imag(k_z)})$ (figure 1(a) right). These three length scales for polaritonic modes are provided in figure 1(d) using the figures of merit $\left(\frac{\lambda_{SPP}}{\lambda_0}, \frac{L_p}{\lambda_{SPP}}\right)$ for doped InAs. One ca notice from figure 1(d) that the ratio of the free-space wavelength (λ_0) and penetration depth (yellow curve) increases asymptotically towards the SPP resonance frequency (here, $\omega_{\rm spp} \approx 27.7~THz$), which indicates the enhanced confinement at this frequency. On the other hand, the ratio of propagation length to SPP wavelength (orange curve) drops significantly near ω_{spp} indicating a substantial propagation loss for the SPP mode.

3. Graphene for infrared optics

Graphene has attracted significant research attention since the initial studies into its properties in exfoliated [2], chemical vapor decomposition (CVD) [87, 88], and epitaxial [3] forms were first reported. Graphene exhibits exceptional optical and electrical properties [2, 89–92], which originate from massless Dirac fermions [93, 94] that serve as the charge carriers, which exhibit high mobility. This results in ballistic carrier transport over micrometers at room temperature in suspended flakes [95, 96]. SPP modes excited in

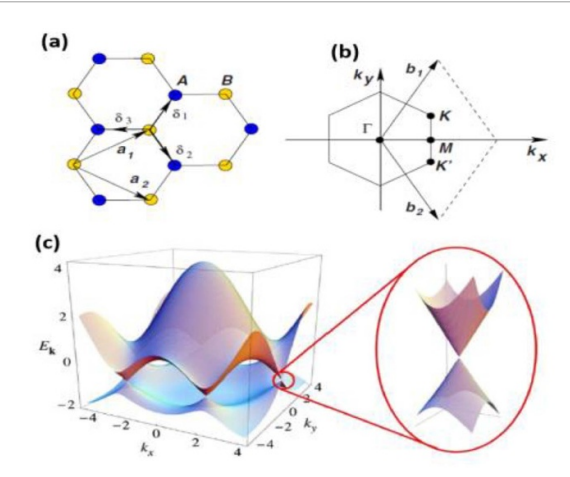


Figure 2. (a) Hexagonal (honeycomb) lattice representation of graphene zone (a_1 and a_2 depict the lattice unit vector while $\delta_{1,2,\text{and }3}$ describe the nearest neighbor vectors). (b) Brillouin zone where K and K' points designate the location of Dirac cones. (c)Electronic dispersion/energy bandgap of graphene showing the Dirac point, with t = 2.7 eV and t' = -2t. Adapted with permission from [111]. Copyright ©2009 American Physical Society.

graphene display superior confinement to those in conventional metals and doped semiconductors, with recent experiments demonstrating the highest reported SPP confinement [29, 97–100]. It also displays relatively low optical losses and can support SPPs throughout the far- to mid-infrared, which makes graphene an exceptional material for plasmonics throughout this spectral range [99, 101, 102]. Moreover, as a 2D material with a zero bandgap (see figure 2 for electronic band structure of graphene), the optical properties of graphene can be altered via electrostatic gating or chemical doping over a broad range of frequencies and thus enables the development of tunable, planar optics [56, 96, 98, 103–110].

With the above-stated properties, graphene has attracted significant research interest for several prospective applications in nanophotonics [103], such as novel solar cells [112–114], optical sensors [115, 116], photodetectors [117–121], ultrafast lasers [116, 122, 123], and many others [24].

3.1. Graphene growth

Several ways to produce graphene have been reported, such as micromechanical exfoliation of single-crystal graphite [2], chemical vapour decomposition on metals and insulators [124–126], unzipping of carbon nanotubes [127], and chemical reduction of graphene oxide [128]. Even though good quality graphene can be produced via most of these synthesis techniques, one of the challenges is that the transfer of the material is required for further processing and device fabrication. In contrast, thermal decomposition of a bulk SiC substrate was introduced as a suitable alternative path to obtain a transfer free, homogeneous, and large-area graphene for electronic and photonic applications [8, 129–131]. This technique consists of subliming Si from the SiC sample at a high temperature $\sim 1400^{\circ}C$ under the vacuum/atmospheric pressure conditions. This results as the vapour pressure of carbon is insignificant compared to the silicon at such temperatures, resulting in the surface carbon atoms reconstructing to form graphitic layers [8, 132] (figure 3(a)).

Ideally, one would benefit from having graphene directly on a silicon substrate for diverse technological applications using conventional CMOS processes. Thus e.g. on 3C-SiC on Si was developed to meet this purpose [3, 8, 9, 133, 134]. The two approaches widely used by researchers to produce e.g. on 3C-SiC on Si are the above mentioned thermal decomposition method (figure 3(b)) [130, 133, 135, 136], as well as metal-mediated approaches that consist of deposition of a metal layer such as nickel or cobalt on 3C-SiC on Si sample followed by heating the sample to the temperature between 700°C to1200°C. Under such conditions, SiC atoms react with the metal layer and form a metal silicide. The carbon atoms released during this process rearrange to the surface throughout the cooling phase to form graphene layers [132, 137, 138].

Furthermore, a catalytic alloying technique for e.g. on SiC on Si was invented [7, 139]. This approach consists of the deposition of a double layer of nickel and copper on 3C-SiC on Si substrate, which followed by heating of the sample at 1100° C for 1 h (figure 3(c)). The removal of excess carbon and metal silicide on the surface of the sample after graphitization is realized through subsequent wet chemical etching, which results in a uniformly distributed graphene on 3C-SiC on Si [140]. Further details about e.g. growth are available in the following references [7, 132, 140, 141].

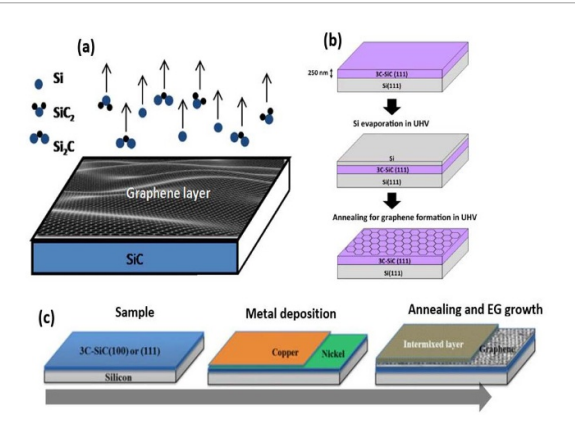


Figure 3. Synthesis of epitaxial graphene (e.g.) on Silicon carbide. (a) Synthesis of e.g. on silicon carbide through thermal decomposition of SiC wafer, Adapted with permission from [132] Copyright © 2016 WILEY-VCH Verlag GmbH & Co. KGaA, Weinheim, (b) Synthesis of e.g. via thermal decomposition of 3C-SiC on a silicon wafer. Adapted with permission from [130] Copyright © 2013 Elsevier, and (c) Growth of EG/3C-SiC on Si via an alloy-mediated catalysis technique. Adapted with permission from [139] Copyright © Materials Research Society 2015.

3.2. Surface plasmon in graphene

The surface conductivity of graphene [30, 142], can be calculated using the well-known Kubo formalism [143, 144].

$$\sigma\left(\mu_{c}, \omega, T, \gamma\right) = \frac{je^{2}(\omega + i2\gamma)}{\pi\hbar^{2}}$$

$$\times \begin{bmatrix} \frac{1}{(\omega + i2\gamma)^{2}} \int_{0}^{\infty} \frac{E\left(\frac{\partial f(E)}{\partial E} - \frac{\partial f(-E)}{\partial E}\right) dE}{0} - \int_{0}^{\infty} \frac{f(-E) - f(E)}{(\omega + i2\gamma)^{2} - 4\left(\frac{E}{\hbar}\right)^{2}} dE \end{bmatrix}$$
(5)

with f(E) describing the Fermi distribution function, which is given by the following expression.

$$f(\mathbf{E}) = \left(1 + e^{\left(\frac{\mathbf{E} - \mu_c}{K_B T}\right)}\right)^{-1} \tag{6}$$

Two distinct solutions result from equation (5), with one expressing intra-band (electron and phonon scattering) contributions, while the other stands for inter-band (bound electron) contributions [145]:

$$\sigma_{\text{intraband}} = j \frac{e^2 k_B T}{\pi \hbar^2 (\omega + i\tau^{-1})} \left[\frac{\mu_c}{k_B T} + 2 \ln \left(e^{\left(\frac{-\mu_c}{k_B T}\right)} + 1 \right) \right]$$
 (7)

$$\sigma_{\text{interband}} = \frac{e^2}{4\hbar} \left[\theta \left(\hbar \omega - 2 \left| \mu_{\text{c}} \right| \right) + \frac{i}{\pi} \ln \left| \frac{\hbar \omega - 2 \left| \mu_{\text{c}} \right|}{\hbar \omega + 2 \left| \mu_{\text{c}} \right|} \right| \right]$$
(8)

where θ ($\hbar\omega - 2|\mu_c|$) defines a step function. The conductivity of graphene can be obtained by summing (7) and (8).

$$\sigma = \sigma_{\text{intraband}} + \sigma_{\text{interband}} \tag{9}$$

For graphene with a carrier density of $\sim 10^{12} {\rm cm}^{-2}$ the intra-band contribution dominates the conductivity of graphene at MIR and far-infrared (FIR) frequencies, while the inter-band contribution dominates graphene conductivity at the near-infrared (NIR) and visible regimes [31]. The effective permittivity of graphene ($\varepsilon_g(\omega)$) can be approximated from its conductivity [146], using equation (9) through the following:

$$\varepsilon_{\mathfrak{g}}(\omega) = \varepsilon_0 + \frac{\mathrm{i}\sigma(\omega)}{\omega\Delta} \tag{10}$$

where Δ describes an effective thickness of the graphene layer.

Similar to conventional plasmonics, a TM polarized wave can be used to excite an SPP mode in graphene. By considering such a wave with the following field components (E_x, H_y, E_z) , one can solve Maxwell's

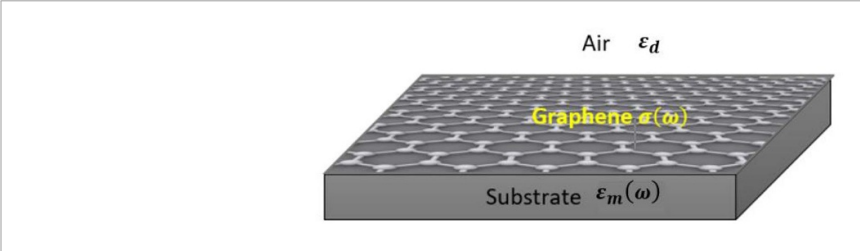


Figure 4. Graphene layer surrounded by air and a substrate of (ε_d) and $\varepsilon_m(\omega)$, respectively.

equations with appropriate boundary conditions to get the following relation for the dispersion of graphene [41, 109].

$$\frac{\varepsilon_d}{\sqrt{k_{spp}^2(\omega) - \varepsilon_d k_0^2}} + \frac{\varepsilon_m(\omega)}{\sqrt{k_{spp}^2(\omega) - \varepsilon_m(\omega)k_0^2}} = -i\frac{\sigma(\omega)}{\omega\varepsilon_0}$$
(11)

where $\sigma(\omega)$ represents the frequency-dependent conductivity of graphene (figure 4).

Equation (11) can be solved to produce the following expression or the dispersion of SPP mode in graphene [41].

$$k_{spp}(\omega) = k_0 \frac{(\varepsilon_d + \varepsilon_m(\omega)) \hbar \omega \left(1 + i(\tau \omega)^{-1}\right)}{4\alpha E_F}$$
(12)

where $\frac{e^2}{4\pi\hbar\epsilon\,\varepsilon_0} \approx \frac{1}{137}$, is the fine structure constant.

In the MIR and FIR spectral regions ($\sim 3 \, \mu m - 300 \, \mu m$), the intra-band transitions dominate the optical behaviour of graphene, causing it to act as a metallic film and support an SPP mode once the sufficient conditions for SPP excitation are fulfilled [147]. Thanks to the 2D nature of collective excitations of carriers in graphene, this SPP mode is confined significantly more than in conventional plasmonic materials, as the wavelength of graphene SPP mode can be much smaller than the wavelength of light at the same frequency [99]. Moreover, exceptional confinement of the SPP mode in graphene can be understood by comparing its dispersion with that of a thin layer of a doped semiconductor (e.g. InAs) of comparable ω_p . The SPP dispersion of a thin-film of InAs can be calculated using the following relation as in [148–150].

$$1 + \frac{\varepsilon_1 k_{z,3}}{\varepsilon_3 k_{z,1}} = j \tan(k_{z,2} d) \left(\frac{\varepsilon_2 k_{z,3}}{\varepsilon_3 k_{z,2}} + \frac{\varepsilon_1 k_{z,2}}{\varepsilon_2 k_{z,1}} \right)$$
 (13)

where d is the film thickness and $k_{z,n}=\left(\frac{\varepsilon_n\omega^2}{c^2}-k_\parallel\right)^{1/2}$ (n = 1, 2, 3) is the longitudinal wavenumber of the SPP supported on the film and the surrounding medium and $k_\parallel\equiv k_{SPP}$. Using the assumption that $\frac{\varepsilon_2\omega^2}{c^2}\ll k_\parallel^2$ [149], we can calculate and compare the dispersion of a 10-nm thick layer of a doped InAs to graphene.

Both graphene and InAs exhibit almost equivalent negative real permittivity values close to ω_p (figure 5(a)). However, a clear deviation can be noticed near this frequency (figure 5(b)), where the k_{SPP} for graphene is much larger than doped InAs near the plasma frequency (55.4 THz). This suggests that SPP modes are more strongly confined in graphene than in doped InAs.

We also used the two figures of merit (FOMs) [151], to compare the performance of doped InAs against graphene qualitatively. The first FOM is associated with the propagation of an SPP mode (FOM_{prop.}), which is given by the L_p normalized to λ_{SPP} , while the second is a measure of the lateral confinement (FOM_{conf.}) of SPP mode at the interface and can be calculated as the ratio between δ_{SPP} and λ_0 .

$$FOM_{prop.} = \frac{L_p}{\lambda_{SPP}} \tag{14}$$

$$FOM_{conf.} = \frac{\lambda_0}{\delta_{SPP}} \tag{15}$$

Graphene displays stronger confinement than InAs of the same ω_p conditions (figure 5(c)). However, in terms of propagation, InAs SPPs do exhibit a larger FOM than graphene. It is worth noting that the relaxation time of t = 8.85 \times 10⁻¹⁴s used in figure 5(c) is low for graphene, but reasonable enough to allow a sensible comparison of its dispersion with that of doped InAs.

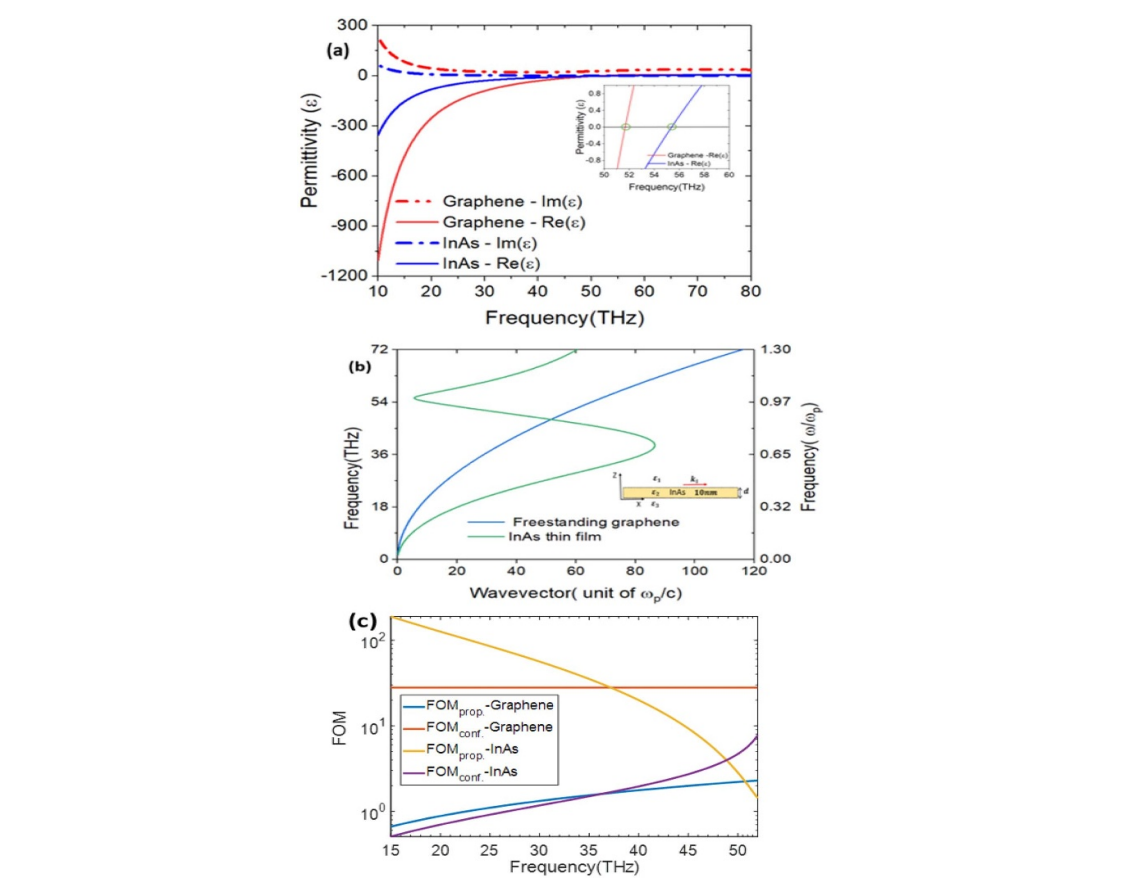


Figure 5. Dispersion relation of SPP in graphene compared with a doped InAs thin film. (a) The calculated permittivity, inset shows the frequency where permittivity is near zero for graphene and InAs. For InAs permittivity is zero at $\omega_p=55.4$ THz. (b) Dispersion relation of SPP modes in both materials. (c) FOM for propagation length and spatial confinement of SPP modes in graphene and doped InAs. The calculation for dispersion relations were performed using equations (1), and (13) for the doped InAs and (10 & 12) for graphene. The ENZ conditions are $E_{F_graphene}=\frac{\omega_{p_finkS}}{2}=27.7$ THz and relaxation time $t=8.85\times10^{-14}s$ for both materials.

Due to the higher polariton confinement of graphene, the 2D material is very promising for the fabrication of novel metamaterial-based devices and nanophotonic applications at the discussed spectral regions [41, 98, 99, 102, 109, 152–154].

3.3. Overview of graphene plasmonics

As discussed specifically for graphene in a number of reviews over the past few years [31, 41, 105, 155], graphene has the major advantage of broad tunability, enabling spectral tuning over much of the MIR to FIR spectral range. While this will be described in this section, it is worth highlighting that recent work has also been able to show exotic physics, such as photodection [156] and emission [157, 158], as well as nonlocality [159–162], and polariton properties controlled by moire lattice formation [163] in stacked layers. This highlights that while graphene plasmonics research has spanned the past decade, there are still new phenomena that are identified regularly within this material. In particular, it is worth highlighting that bilayer graphene may also hold many benefits in terms of infrared optoelectronics [155, 164, 165]. However, for the purpose of this review, we will focus on the tunable properties of graphene plasmons as it pertains to their interactions with silicon carbide.

3.3.1. Tunability of surface plasmon polariton in graphene

The linear dispersion of the Dirac fermions in graphene is the basis of its broadband tunability, which makes it superior to other plasmonic materials [41]. Typically, the charge carriers induced in graphene through doping can be increased from on the order of 10^{11} cm⁻² to 10^{13} cm⁻² [166]. Pradeep *et al* using Hall effect measurements have recently reported carrier concentrations exceeding such values, reporting 3×10^{13} cm⁻² and 7×10^{13} cm⁻² for e.g. on SiC/Si(100) and e.g. on SiC/Si(111), respectively [167]. Additionally, the carrier concentration in graphene can be increased up to 10^{14} cm⁻² through electrostatic gating [168]. Such broad tunability has enabled the realization of numerous novel photonic devices and applications, such as tunable signal modulators [169–174], optical detectors [98, 121, 175, 176], and filters [177, 178] along with

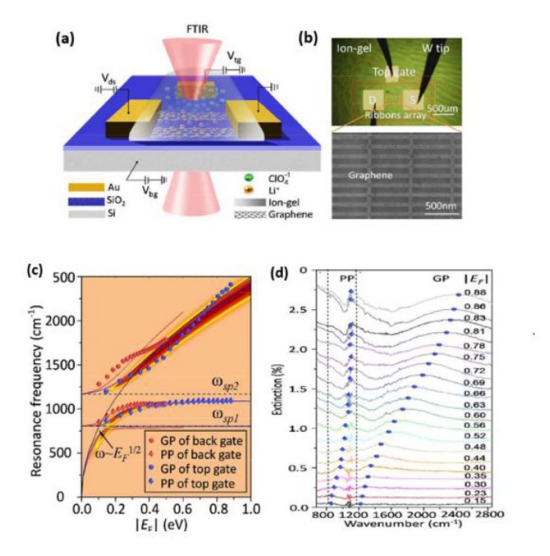


Figure 6. Hu *et al* work on graphene tunable plasmons [188]. (a) The diagram of the experiment set up for graphene plasmon tunable device, (b) top image shows an optical micrograph of the fabricated graphene nanoribbon device covered with ion gel (green), and the bottom is an SEM image of graphene nanoribbon array. (c) the calculated resonance frequencies of phonon like polariton (PP) and graphene' plasmon (GP) peaks as a function of Fermi energy controlled through the top gate (blue curves) and through the back (red curves), diamond and spheres curves denote experimental results. (d) extinction spectra of the graphene nanoribbon array at different values of Fermi energy tuned through the top ion gel. Adapted with permission from [188] Copyright © Royal Society of Chemistry 2015.

many others. As previously shown in equations (5)–(12), both the conductivity and SPP dispersion of graphene depends directly upon the Fermi energy, but are also strongly sensitive to the nature of the surrounding dielectric environment, frequency, electronic band structure, and densities of states of the carriers [31]. For monolayer graphene, the Fermi energy can be calculated as: $E_F = \sqrt{\pi \hbar^2 v_F^2 n}$, where \hbar represents the reduced Planck constant, while v_F and n represent the graphene Fermi velocity ($\approx 10^6 \frac{m}{s}$) and carrier concentration, respectively. Thus, the control of the carrier density can be simply represented via the Fermi energy in EG [179, 180] and free-standing graphene [181–183]. The roughness of the SiC film on which e.g. is formed can affect carrier mobility, with a roughness of about 1 nm RMS required for good-quality e.g. [132, 184]. Other factors that impact the intrinsic properties of e.g. are crystallographic defects, such as anti-phase boundaries [185], which are more prevalent in thinner films [186, 187].

Due to the strong sensitivity to local materials and interfaces in the proximity of graphene, these changes in the environment can induce doping in graphene through charge transfer processes, where p-doping can result from polymers with nitrogen, fluorine, and oxygen constituents, while n-doping can be induced in graphene on metallic samples [31]. Thus, careful materials selection is needed to control the carrier density and doping and thus has become one of the most common practices in controlling its electronic properties. For example, Hu *et al* demonstrated the use of an ion-gel to induce a broadly tunable SPP mode at a fixed frequency of 1270 cm⁻¹ using low voltage modulation of about 4 V tuned from the Dirac point [188] (see figure 6). Furthermore, by encapsulating graphene between layers of hexagonal boron nitride, it is possible to maximize the propagation length [97]. Further works concerning graphene SPP tunability can be found in these references [99, 105–107, 189–192].

However, one of the advantages of having graphene grown directly on SiC in the context of nanophotonics is that the graphene SPPs can couple directly with SPhPs supported in the underlying SiC within the long-wave IR. Within a spectral range between approximately 10.3 to 12.5 μ m a hybrid mode can be formed with enabling properties, such as robust confinement, and broad spectral tunability [193–195]. However, before we discuss such hybridization, let us start by providing an overview of the fundamentals governing the excitation of the SPhPs in polar dielectric materials. In the next section, we discuss the physics behind the excitation of SPhPs in SiC and the application of these modes for nanophotonics.

4. Surface phonon polaritons in silicon carbide

While SPPs are derived from the coupling of coherent free-carrier oscillations with light, the collective ionic oscillations of a polar crystal enable the stimulation of SPhPs [23, 27]. These modes are analogous to SPPs and can be supported within the spectral region known as the Reststrahlen band [84, 196], which is bound between longitudinal (LO) and transverse optic phonon (TO) frequencies [197]. SPhP modes have been

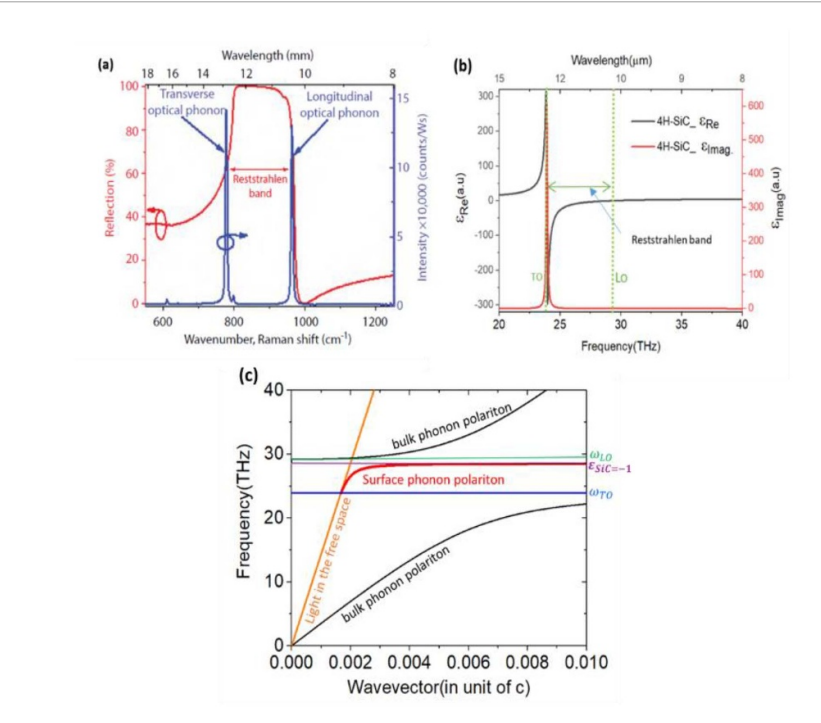


Figure 7. (a) Measured FT-IR spectra (red curve) of 4H-SiC indicates the high reflectivity nature of SiC within the Reststrahlen band, while the Raman spectra indicate the positions of optical phonon modes [27]. (b) The calculated dielectric function of 4H-SiC showing real and imaginary permittivity, the broken vertical black lines indicate the position of TO (left at 23.9*THz*) and LO (right at 29.2*THz*) frequency, the two parallel vertical dashed lines(LO and TO) represent the Reststrahlen band, (c) Dispersion of surface phonon in 4H-SiC, and light is propagating in free space calculated using relation(4). The calculation was performed using 4H-SiC data for 4H-SiC $ω_{To} = 797$ cm⁻¹(23.9 *THz*) $ω_{To} = 973$ cm⁻¹(29.2 THz), and $\Gamma = 4.7$ cm⁻¹(0.1 *THz*) [27].

demonstrated in a wide variety of polar materials such as SiO₂ [198], GaAs [199, 200], SiC [197, 201], hexagonal [202, 203] and cubic BN [204], and revealed strong field (sub-diffraction) confinement with relatively low optical losses [23]. Moreover, due to the optic phonon nature of SPhP modes, they are resonant in the MIR to THz spectral ranges, a region of great interest for applications in thermal imaging and chemical spectroscopy. Above all, SPhP modes have been reported with high resonance quality factors of up to 300 in the far-field, and 400 in the nearfield with long lifetimes on the order of one to hundreds of picoseconds [205, 206], with a very recent record high-quality factor of 501 realized in hBN [207]. This is in comparison to SPPs, which feature quality factors typically on the order of 10, resulting from scattering lifetimes of tens to a few hundred femtoseconds [32, 197]. These effects thus identify polar dielectrics as low—loss materials compared to their SPP counterparts [27, 84, 197]. In the following section, we discuss the dispersion of SPhP modes using SiC as a case study.

4.1. Dispersion of surface phonon polariton in silicon carbide

In order to understand the physics associated with the excitation of SPhP modes in SiC, it is worthwhile to look back on the optical properties and phenomena that cause metals to support SPPs. Similar to metals, polar dielectric materials also exhibit high reflectivity and negative real part of the permittivity within the Reststrahlen band (figures 7(a)–(b)) [27, 208]. The dielectric function of such polar materials thus deviates from Drude materials (e.g. metals and doped semiconductors) in that the negative permittivity is only observed within the Reststrahlen band, and thus is typically defined by the so-called TOLO formalism provided in equation (16):

$$\varepsilon(\omega) = \varepsilon_{\infty} \left(1 + \frac{\omega_{\text{Lo}}^2 - \omega_{\text{To}}^2}{\omega_{\text{To}}^2 - \omega^2 - i\,\omega} \right) \tag{16}$$

where ω_{TO} and ω_{LO} , represent the TO and LO phonon frequencies, respectively, while Γ defines the damping constant associated with optic phonon modes, respectively.

A plane wave incident on the surface of a polar material may stimulate an evanescent wave within the Reststrahlen band, provided methods for overcoming the momentum mismatch between the incident free-space light and the polaritonic mode are employed as described previously [38].

4.2. Silicon carbide nanophotonics

Analogous to plasmonic materials, the surface of SiC can be carefully tailored, and nanostructure patterns fabricated into it that can support long-lived localized SPhP modes [209–214]. These SPhPs are known to be tightly confined at subwavelength scales and exhibit high-quality factors with expected Purcell enhancements on the order of about three order magnitudes higher than what is attainable with noble-metal and doped semiconductor plasmonic structures [197, 215]. Furthermore, akin to plasmonics, nanoscale patterning of SiC can also be employed to induce gratings and thereby enable phase matching for excitation of propagating modes [210]. The ability to couple localized resonances with propagating modes in SiC has been proposed as a means to realize photonic integrated systems similar to those with SPP modes [216]. One such hybrid localized/propagating SPhP mode is the so-called monopole resonance that results from a coupling between a propagating SPhP and a modified longitudinal dipole when nanostructures are fabricated into the same polaritonic material [32, 217–221]

Feldman [222, 223] was the pioneer in developing our understanding of optic phonons within SiC, with Nienhaus [201] and Nakashima and Harima [224] extending our understanding substantially when they revealed excitation of surface phonons in 3 C, 4 H and 6 H-SiC using Auger electron spectroscopy, high-resolution electron energy loss spectroscopy and with Raman scattering techniques. Tiwald et al [225] reported a widely employed dielectric function model for SiC that subsequently enabled the seminal works of Hillenbrand et al [226]. and Greffet et al [227], which revealed the first experimental studies of SPhPs in this material. Hillenbrand et al [226] used scanning near field optical microscopy (SNOM) to investigate propagating SPhPs on 4 H-SiC surfaces. By mapping the spatial amplitude (proportional to reflection) and phase (absorption) of the infrared optical response of the material resulting from the scattering of incident infrared laser light off of a metalized atomic force microscope tip near the SiC surface, they revealed a contrast in the near field amplitude of the sample at frequencies within the Reststrahlen band. This is shown in figures 8(a)-(c), where the brightness of the SNOM image displays enhancement in the scattering amplitude of incident optical fields on the surface of 4 H-SiC in comparison to the surrounding Au. At the same time, Greffet et al [227], used SiC-based gratings to induce spatially coherent thermal emission (figures 8(d)–(e)). This was followed by Taubner et al exploring superlenses in the near field [213] and additional work from the Shvets group, which demonstrated prism coupling for chemical sensing platforms [228, 229].

Subsequently, Schuller et al demonstrated that far-field measurements of the resonant localized modes [214], and that they could serve as the basis for a polarized narrowband IR thermal source [230]. Caldwell et al demonstrated the wide flexibility and tunability of silicon carbide-based nano-antennas, where they explored sub-diffractional, localized SPhPs in nanopillar arrays fabricated in 6 H-SiC [197]. Extraordinarily narrow resonance linewidths (ranging from 4 to 24 cm^{-1}), were reported, with corresponding quality factors of about 40 to 135, which exceeded typical values in pure plasmonic resonators by about an order of magnitude (figures 9(a)–(c)). Similarly, Wang et al demonstrated the ability to realized resonant SPhP modes through creating metal apertures on the surface of SiC, which offered quality factors as high as 60 [231]. More recently, quality factors of a few hundred have since been reported in this material system [232, 233]. The model reported by Caldwell et al [197] revealed coupling of the localized SPhP modes to extremely small modal volumes $\sim \left(\frac{\lambda_{\text{reso}}^3}{V_{\text{effect}}}\right)^{\frac{1}{3}}$, which yielded potential Purcell enhancements of 1.9×10^6 to 6.4×10^7 , far larger than what can be theoretically realized with SPPs. Furthermore, in work by Chen et al [232], they reported that the resonance intensities remain almost unaffected irrespective of variation in the filling fraction of the nanopillars, resulting from the strong coupling between the localized and propagating SPhPs supported in this system. Gubbin et al (2016), built on this work, investigating the strong coupling, localization, and propagation of SPhP modes in SiC-based resonators (cylinders of micron size) [210]. In their study, the nanoresonators were fabricated into SiC wafers to induce the localized SPhP modes and to act as grating coupler for excitation of propagating SPhPs (figures 9(d)-(f)). From the tunability of the SPhP dispersion, they found a spectral anti-crossing occurred between localized and propagating modes, which confirmed strong coupling between them. It is worth noting that such an anti-crossing is only achievable if the Rabi frequency (oscillation frequency of a Rabi cycle undertaken for a given atomic transition in a given EM field) exceeds the losses of the combined modes [234].

Recently, Gubbin *et al* used 4 H-SiC nanopillars to demonstrate strong coupling between transverse and longitudinal SPhPs and theoretically modelled this behaviour through the realization of hybrid excitations referred to as longitudinal-transverse-phonon-polaritons (LTPP). These strongly coupled modes were observed experimentally by tuning localized SPhP monopolar resonance into the spectral proximity of a zone-folded LO phonon intrinsic in SiC polytypes with higher degrees of hexagonality [235]. Such coupling between longitudinal and transverse fields offers the potential opportunity to electrically stimulate optically active modes, with their work paving the way towards the development of novel MIR emitters. Similarly, Folland *et al* recently demonstrated that SPhPs in SiC could couple to molecular vibrational transitions in a

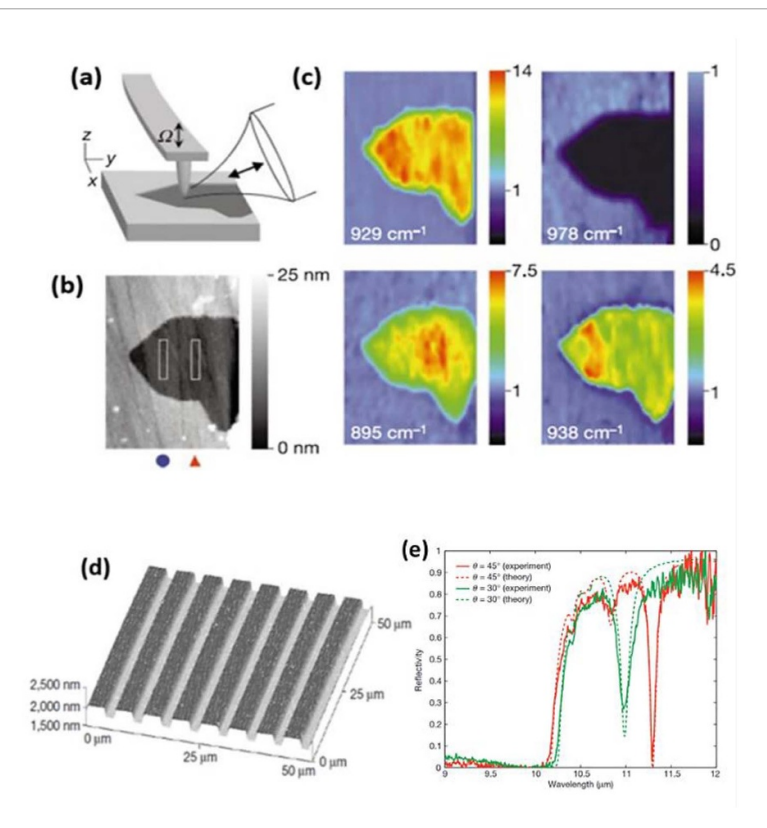


Figure 8. Experimental works on the propagating SPhP mode in SiC. (a) Probing of phonon in SiC using scattering-type MIR scanning near field microscopy(s-SNOM). (b) Image of Au covering SiC sample (2 rectangles shows the area used to extract the data. (c) The infrared near field images showing the scattering field amplitude taken at different illumination frequencies (the blue colour shows Au). SiC surface looks much brighter than other areas covered by Au at the phonon resonance frequency (929 cm⁻¹). The contrast reverses at 938 cm⁻¹. IR images taken from either side of the phonon resonance show a systematic local variation at 895 cm⁻¹ and 938 cm⁻¹. (d) Atomic force microscopy image of SiC-based grating to support SPhP. The period of grating $d = 0.55\lambda$ ($\lambda = 11.46 \ \mu m$) was taken so that the propagating surface wave could couple with the propagating wave at the frequencies at the studied frequencies. (e) Measured and calculated reflectance of SiC grating at the MIR, Showing the dependence of SPhP response on the incident angle. (a–c) adapted with permission from [226] Copyright © 2002, Springer, and (d & e) adapted with permission from [227] Copyright © 2002, Springer.

liquid, paving the way for a new methodology for creating vibrational polaritons and strong coupling in a liquids [236]. Further opportunities for ultrafast modulation of SPhPs was demonstrated by Dunkelberger *et al* through the injection of free carriers into localized SPhP resonators [237].

Nevertheless, the challenges associated with excitation of the SPhP modes in polar materials are that their responses are limited to the narrow, material-specific Reststrahlen bands, which hinders the exploitation of these modes over a broad frequency ranges [208, 238]. Further, the fast spectral dispersion in the dielectric function within this band also infers that the SPhPs will result in modes with exceptionally slow group velocities, thereby limiting propagation lengths despite the long polariton lifetimes [27]. While efforts to overcome such limitations are underway via the crystalline hybrid concept [239], these challenges remains a significant roadblock. On the other hand, the experiment conducted by combining polar materials with graphene has revealed an ability to overcome the restrictions of SPPs and SPhPs through the electromagnetic hybrid concept [239], which relies on the formation of phonon-plasmon hybrid modes [22, 194, 240–243]. These experiments demonstrate the possibility to develop devices with low-losses as a result of the long lifetimes of SPhPs and the broad spectral tenability of graphene SPPs. For instance, hybrid SPP-SPhP modes in graphene and hBN were demonstrated to propagate longer than the pure polaritons in either material [244]. Moreover, the coupling of graphene SPPs with SPhPs in polar materials is supported by the recent advancement in synthesis techniques, which enabled graphene to be grown directly on a given substrate, perhaps most importantly on silicon [130, 139, 140]. In the following section, we will review the current literature as it pertains to hybrid SPP-SPhP modes within graphene on silicon carbide heterojunctions.

5. Hybrid phonon-plasmon polaritons in graphene on polar materials

One of the essential aspects of graphene is that it can couple strongly to the various dielectric substrates for diverse applications [170]. However, one of the biggest challenges is to maintain its exotic properties while

J. Phys. Mater. 3 (2020) 032005 P Rufangura et al

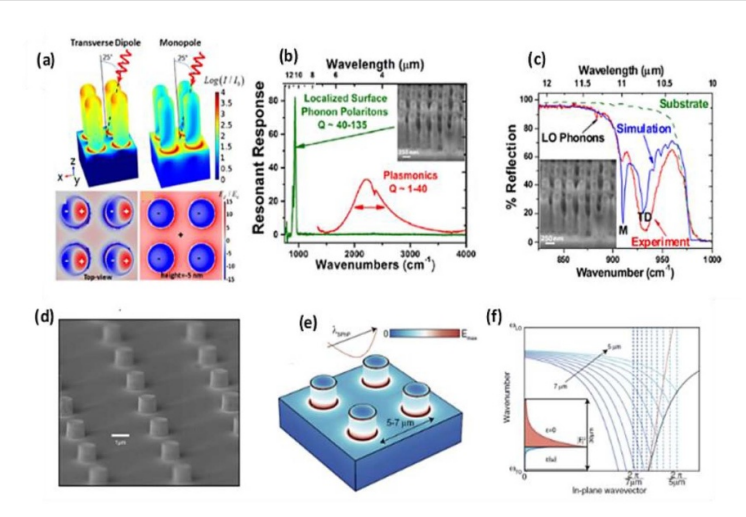


Figure 9. Excitation of localized SPhP in SiC. (a) The profiles of the field distributions in SiC-based nanopillars with contributions due to the transverse dipole and monopole modes. (b) depicts the spectral resonant responses of 6H-SiC-based nanopillars with a comparison between Q factor of plasmonics mode (in plasmonic materials) and localized SPhP modes (in polar dielectric materials) for 6H-SiC, Inset shows arrays of 6H-SiC-based nanopillars. (c) FTIR reflectance spectra of the periodic array on 6H-SiC with the simulation results of the nanopillars showing the monopole(M) and transverse dipole(TD) resonances of the SiC-based device. (d) SEM image of a SiC device fabricated to excite localized SPhPs modes. (e) Electric field norm for the modes of the coupled array with the sinusoid curve to show the SPhP mode wavelength. (f) Dispersion of the SPhP mode (black curve), the solid blue line show SPhP mode folding from the edge of the first Brillouin zone for different periodicities varying from 5–7 μ m, while the inset shows the norm of the electric field of the SPhP mode at air/SiC interface. (a–c)adapted with permission from [197], Copyright © 2013 American Chemical Society. (d-f) Adapted with permission from [210], © 2016 American Physical Society.

transferring it onto those substrates (most of the synthesis techniques are built on ex-situ growth where the transfer of graphene flakes is required for device fabrication and characterization) [132]. For instance, suspended single-layer graphene can have carrier mobilities of about 200.000 $cm^2V^{-1}s^{-1}$, but this mobility drops considerably once graphene is placed on a dielectric or an insulating substrate such as SiO₂ [95]. Surface optic phonons from the dielectric substrate induce increased scattering of the free carriers in graphene and serve as one of the predominant factors limiting the carrier mobility. This can be mitigated by placing graphene on an appropriate substrate, such as hBN [97, 244], where the mobility can be much higher.

As discussed previously, different ways to synthesize e.g. on silicon carbide on silicon have been developed [132, 133, 140]. The essential advantage of this growth technique is that the graphene layers are directly grown on the substrate. Thus, no transfer is required for optical/electrical characterization and device fabrication, which prevents damage to the graphene layers, eliminates deleterious effects from residual polymers, and thus provides the most straightforward avenue towards maintaining the intrinsic properties of graphene.

This is a benefit for the development of EG-based photonic devices (e.g. photonic crystal cavities) on SiC on Si, thanks to the well-established silicon fabrication techniques and scalability [245, 246]. Moreover, one can optimize the geometry of this heteroepitaxial system containing graphene and SiC on Si to couple their SPP-SPhP modes. To understand this coupling within the EG/SiC system, in the following section, we analyze the dispersion relation for epitaxial graphene on SiC.

5.1. Dispersion of hybrid phonon-plasmon mode in epitaxial graphene on silicon carbide

Much of the physics of hybrid SPP-SPhP within the EG/SiC system can be extracted from the dispersion relation of this material system. To analyze the effect of coupling, however, it is worth looking back to the dispersion of each material involved in the coupling. As discussed earlier, the dispersion of the large wavevectors of SPP modes in graphene at frequencies approaching the plasma frequency results in a large momentum mismatch with free-space light. This results in extremely short polariton wavelengths and, thus, strong field confinement of SPPs in graphene. On the other hand, the dispersion curve of SPhPs in SiC coincides with the light line at the TO phonon and asymptotically approaches large momentum values near the LO phonon (figure 10(b)). Hwang *et al* realized that hybridization between graphene and SiC polaritons modifies their dispersion curves [242], where two different energy regions arise (symbolized by ω_+ and ω_-) separated by a gap (forbidden zone) between surface optic phonon frequency (ω_{SO}) and ω_{TO} [194, 242]. ω_{SO} defines the asymptotic limit over which the optic phonon mode can be stimulated on a planar surface, and it is related to ω_{TO} as $\omega_{SO} = \omega_{TO} \sqrt{\frac{\varepsilon_s + 1}{\varepsilon_\infty + 1}}$ [242], where ε_{st} and ε_∞ define the static and high-frequency

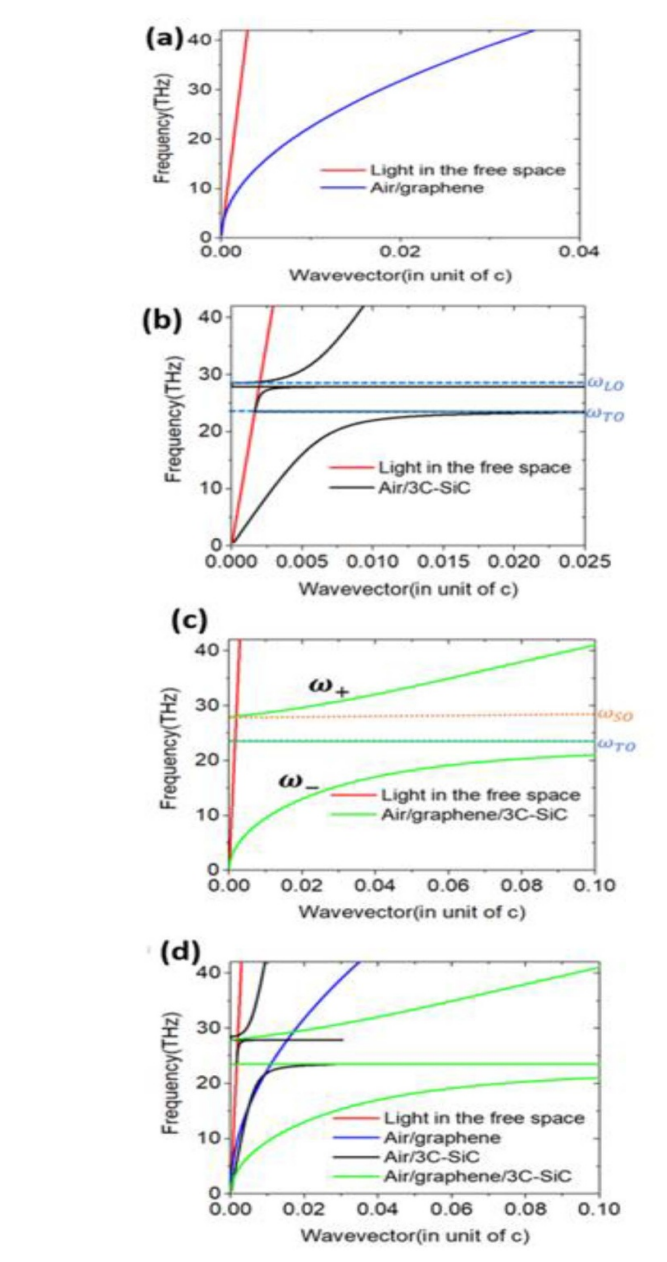


Figure 10. Dispersion relation of (a) SPP in the free-standing graphene (b) the dispersion of phonon polariton in a free-standing 3C-SiC. (c) The hybrid phonon-plasmon mode in air/graphene/3C-SiC material system (ω_+ and ω_- Show the two regions resulting from the coupling between SPP mode in graphene and SPhP mode of 3C-SiC). (d) A comparison between the dispersion curve of free-standing graphene (blue), 3C-SiC (black curve), and air/graphene/3C-SiC (green curve) system. The wave vector is normalized to the speed of light in the free space 'c.' The calculation for the dispersion graphene on SiC was performed using equation (12) with Fermi energy $E_F = 1eV(245\ THz)$ and dielectric properties data for 3C-SiC $\omega_{LO} = 118meV(28.5\ THz)$ and $\omega_{TO} = 97.3meV(23.5\ THz)$ and $\Gamma = 0.6meV(0.1\ THz)$ [27].

dielectric constants of the material, respectively. One can notice from figure 10(c) that for lower frequencies the wavevector of the hybrid system drops towards zero $(k \to 0)$, with the modes in the lower region (ω_-) behaving more like SPP modes, while those in the upper region (ω_+) exhibiting characteristics more akin to the SPhPs and converge towards surface optic phonon frequency $(\omega_+ \to \omega_{SO})$. On the other hand, for higher wavevectors $(k \to \infty)$ the mode in the lower region (ω_-) converges towards ω_{TO} and behaves more like SPhP mode, (see figure 10(b) for SPhP dispersion in 3C-SiC), while the modes in the upper ω_+ region exhibit SPP-like features (figure 10(a)). These can be understood from the strong coupling between SPhPs supported in the substrate and the collective SPP mode and electronic degrees of freedom in graphene [41]. Note that the green lines for the dispersion curve of graphene/3C-SiC differ from the bulk phonon polariton observed in SiC, and this is because of the presence of graphene [194, 242].

5.2. Graphene on silicon carbide photonics

The successful synthesis of e.g. on 3C-SiC/Si wafers was a substantial leap forward as such a system enabled large area and uniform growth of graphene on a desirable substrate, which benefits the advancement of photonic and electronic research fields [3, 247]. SiC has been used in micro/nano-electronics for many years, and studies on growing pristine graphene on different polytypes of SiC have been conducted for more than a decade [3, 132]. However, there is still a need to get further insights into the interactions between graphene and SiC, such as carrier dynamics that can be affected by the range of coupling and interference effects that result from optic-phonon/free-carrier interactions. Recent progress in obtaining graphene from hetero-epitaxial 3C-SiC on silicon [7, 130, 140], holds promise for potentially adopting and translating this powerful approach to create a platform for nanophotonics in a silicon-compatible material system.

A study investigating the coupling of SPP and SPhP modes in epitaxial graphene on SiC was conducted using dispersion measurements via angle-resolved electron energy loss spectroscopy (AREELS)" [243]. In this work, graphene was epitaxially synthesized on a 6H-SiC (0001) substrate. AREELS measurements were performed on epitaxial graphene and bare hydrogen (H)-etched SiC (6 H-SiC (0001)) at room temperature and a pressure of 2×10^{-10} torr. Robust coupling of about 130 meV (much higher than 20 meV measured from the coupling of the SPP to SPhP modes in GaAs [248]) was observed between the dipolar E fields [249]. This coupling originated from the collective oscillation of π -electron charges in graphene and the collective vibrations of SiC. The carrier density of graphene was recorded to be in the range of 10¹³ cm⁻² as a result of the charge transferred from the surface of SiC to the graphene sheet [243]. The momentum of phonon modes in SiC caused these transferred charges to oscillate, a phenomenon which is understood to be the source of unusually strong anti-crossings observed in the measured dispersion curve of the coupled system (see figure 11(a)). Subsequently, Kosh, Seyller & Schaefer, conducted another study about plasmon and phonon coupling where high-resolution electron energy loss spectroscopy (HREELS) was utilized to reveal strong coupling of these modes in graphene on 6 H-SiC (0001) with a higher carrier density in the range of 1.5×10^{15} cm⁻³ at the long wavelength limit [194]. The spectra of energy loss recorded (see figure 11(b)) confirmed the existence of coupled plasmon and phonon modes separated by ω_{50} and ω_{70} . Coupling was also theoretically confirmed in figure 11(c), whereby using the dielectric function, the spectra of the energy losses, and dispersion of the two coupled modes was calculated. Later, Kosh et al again realized the coupled phonon-plasmon modes in e.g. on SiC [193]. In their study, they used HREELS and a dielectric function model to unveil coupling for epitaxial graphene to the buffer layer and in quasi-freestanding graphene on both oxygen and hydrogen-intercalated SiC (0001) (See figures 11(d)-(f)). They revealed the coupling of internal modes to occur even for bilayer graphene with asymmetric inversion, which results from disparity of charges across the layers. They also revealed that interface modification through intercalation cannot quench plasmon-phonon coupling in the e.g. on SiC substrate.

Moreover, the strong coupling of SPPs to localized SPhP modes in graphene and periodic gratings (micro-cavities) fabricated into SiC substrates (to induce localized and propagating modes in the system) was theoretically studied for tunable SPPs at infrared frequencies [250]. In that study, they considered monolayer graphene on a SiC grating, and they used numerical calculations with the finite element method (FEM) [251] to investigate the optical responses. It was reported that as SiC will behave as a near-perfect reflector within the Reststrahlen band, this can enable a cavity effect sufficient to launch graphene SPP standing waves [208]. Rabi splitting in the absorption spectra confirmed the presence of strong coupling of the localized SPhP resonant modes supported on the SiC grating and SPP resonances in graphene cavity modes. The resultant hybrid mode displayed the characteristics of each constituent (SPPs in graphene and SPhPs modes in SiC). The tunability of the mode in their device was also revealed by varying the chemical potential of graphene, and by changing the cavity width, where they observed a shift in absorption peaks. Moreover, Qing et al [174], theoretically demonstrated that an ultrathin layer of MoS₂ and hBN sandwiched between SiC and graphene can support extremely confined SPhPs with confinement factors over 100 and a tunable hybrid SPP-SPhP mode which was used for an electro-optic modulator with over 95% of modulation depth. Further works on the hybrid coupling of the SPP-SPhP modes in e.g. on SiC were performed in the following references [195, 241, 252–254].

5.3. Propagation and spatial confinement of hybrid SPP-SPhP mode in graphene on silicon carbide

As previously discussed in section 2, the propagation length and the degree of confinement of SPP/SPhP modes have a considerable influence on their use in diverse photonics applications. However, it is not easy to find a plasmonic material with low propagation losses and strong confinement simultaneously. For example, the strong spatial confinement of graphene SPPs via the extremely short polariton wavelengths are understood to be limiting its propagation length to few tens of microns [255] and affects its use for some of the applications where long propagation lengths are required, such as in information processing and communications [256, 257]. As mentioned previously, the long lifetimes of SPhP modes do not necessarily

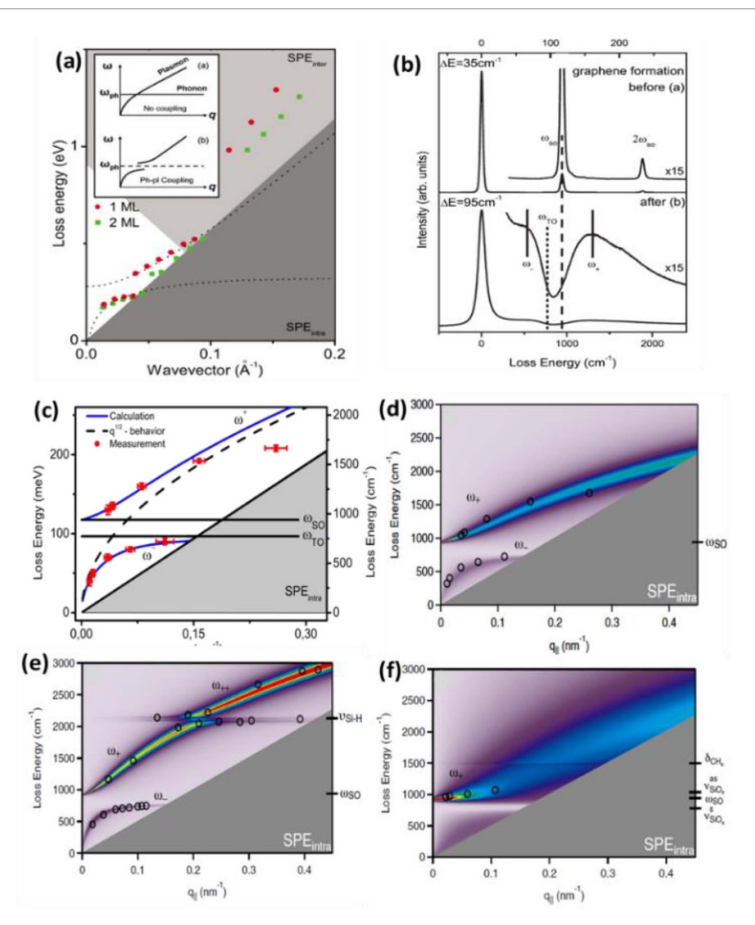


Figure 11. (a) Graphical representation of the peaks energy losses against wave vector in monolayer (ML) and bilayer graphene on SiC. The dashed surfaces show the area covered by single-particle excitation (SPEs) spectrum results from inter-band and intra-band transitions while the two inset show plasmon and phonon modes before(top) and after coupling (bottom), adapted with permission from [243]. ©2010 American Physical Society. (b) Spectra of energy loss (measured by HREELS at the resolution of 20 cm⁻¹) of hydrogen etched SiC (before graphene formation on top) and on e.g. SiC (001) after formation of graphene (bottom curve), (c) dispersion of SPhP-SPP modes coupled (red dots and solid blue lines represent measured and calculated results, respectively. The dashed line describes the nature of $q^{1/2}$), b &c adapted with permission from [194]. ©2010 American Physical Society. (d) Dispersion of plasmon-phonon coupled modes on monolayer graphene on SiC, (e) dispersion of plasmon-phonon coupled modes for oxygen terminated e.g. on SiC (0001) and (f) dispersion of plasmon-phonon modes and are marked by ω_- , ω_+ and ω_{++} while the back and white circles indicate the maximum energy losses as measured with HREELS recorded at different primary beam energies. (d–f)adapted with permission from [193]. © 2016 American Physical Society.

result in commensurate increases in propagation lengths, with typical values reported falling in a range that is of an order comparable to that for SPPs [27, 238, 258].

To quantify the properties of the hybrid graphene/SiC material system, we used equations (14) and (15), and calculated FOMs for graphene SPP and SiC SPhP modes and compared them with that of the hybrid SPP-SPhP mode (figure 12). While SiC along exhibits a slightly higher FOM in comparison to graphene SPPs (figure 12(a)), graphene outperforms SiC SPhPs in terms of spatial confinement (figure 12(b)). One can notice that the hybrid graphene/SiC polaritons provide an improved FOM for spatial confinement in comparison to those of the individual materials (yellow and purple curves in figure 12(b)). However, the propagation FOM for the SPP-SPhP mode in the hybrid graphene on SiC system seems to be not as good as the FOMs of the individual SPP and SPhP modes in SiC and graphene (figure 12(a)). As reported by Lu et al, FOMs for propagation and spatial confinement can be further improved by adjusting the chemical potential or carrier density in graphene [255]. For instance, by increasing the carrier density in graphene from 1×10^{12} cm⁻² (used in the calculation for yellow curves in figure 12) to 1×10^{13} cm⁻² (and mobility of $\sim 100 \frac{\text{cm}^2}{\text{Vs}}$ as reported in [167] for graphene/SiC system), we can improve the propagation at the expense of the confinement FOMs of hybrid SPP-SPhP mode in graphene on SiC system (purple curves in figure 12). Note that the improved FOM for propagating hybrid SPP-SPhP mode occurs near to ω_{TO} (\sim 23.5 THz) and at the frequency ~28THz (within the Reststrahlen band), the spectral position where SPhP mode in SiC can couple with graphene's SPP mode (see purple curve in figure 12(a)).

Such improvements of SPP-SPhP modes was experimentally revealed for graphene coupled to hBN, which resulted in extended propagation lengths for the hybrid mode that were 1.5–2.0 times longer than the

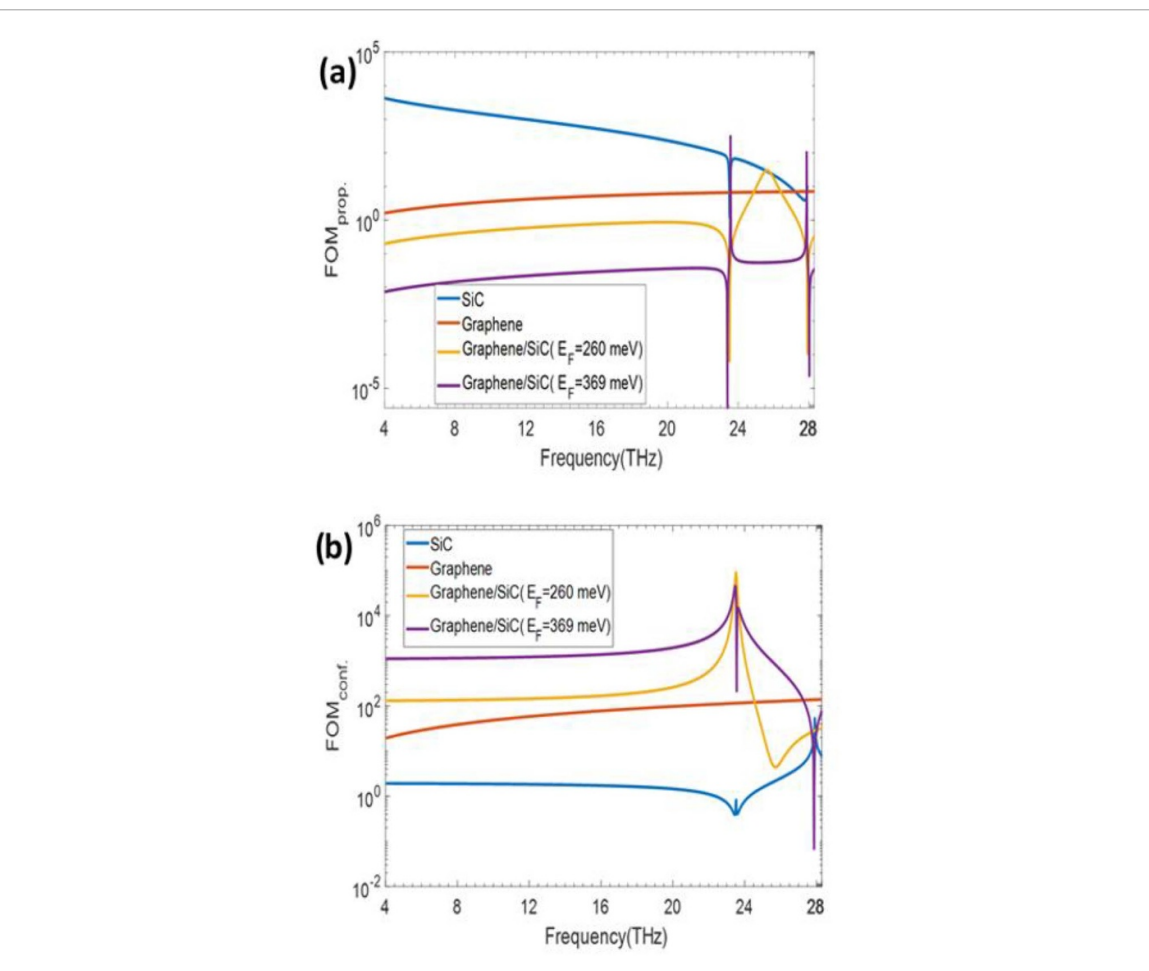


Figure 12. FOMs for graphene, SiC, and graphene on SiC. (a) FOM for the propagating mode (ratio of propagation length and wavelength of SPP or SPhP mode) (b) FOM for the lateral confinement of the modes (ratio of the free space wavelength and evanescent field decay in the air from air/plasmonic or phononic material interface). The yellow and purple curves show that the propagating and lateral confinement FOMs of the hybrid polariton modes in the graphene/SiC system can be improved by tuning the Fermi energy in graphene. The calculations were performed using $E_F = 260 meV (n \approx 1 \times 10^{12} cm^{-2})$ with relaxation time $\tau = 261 fs$, and $E_F = 369 meV (n \approx 1 \times 0^{13} cm^{-2})$ with $\tau = 4 fs$. The dielectric properties data for 3C-SiC used here are $\omega_{LO} = 118 meV (28.5 THz)$, $\omega_{TO} = 97.3 meV (23.5 THz)$, and $\Gamma = 0.6 meV (0.1 THz)$ [27].

individual modes [238, 244]. Furthermore, This offers the opportunity to increase the propagation or lateral confinement depending on the desired applications.

6. Conclusions and outlook

The sub-diffractional confinement of light offered by the hybridization of SPPs and SPhPs is a very promising gateway to further advancement of photonic integrated systems. However, in order to realize sub-diffraction photonics for any anticipated applications, the choice of the constituent materials and tailoring of the operational spectrum are two critical factors that need special consideration. Photonic systems with low optical losses and dynamically tunable can offer a broader range of spectral and function flexibility, and graphene can offer such opportunities while supporting tightly confined optical fields. The coupling of graphene with polar materials that support low loss SPhPs offers further opportunities to improve the loss characteristics beyond what is achievable in graphene SPPs alone in MIR and FIR frequencies. Thus, we note that realization of high performance (low optical losses and tunable) nanophotonic systems could be best achieved via a tailored combination of multiple materials to generate electromagnetic hybrid modes in a device. For example, such strongly coupled modes could offer the opportunity for electrically driven, narrow-band optical modulators or emitters.

While in most instances strong coupling between SPPs in graphene with SPhPs in polar substrates requires the graphene to be mechanically transferred [132, 259, 260], e.g. offers the opportunity to realize epitaxially grown graphene directly on SiC [3, 9, 261], offering unique opportunities to couple tunable graphene SPPs with long-lifetime SPhPs in SiC in a single versatile optical platform. Here we reported that such a combination can actually improve the propagation length and spatial confinement simultaneously for

these hybrid modes over the individual constituents, offering additional benefits for nanophotonic applications and device designs; however, this requires that experimental works be conducted to validate this prediction.

This recent progress in the quality and control of epitaxial graphene on hexagonal SiC wafers and cubic SiC on silicon opens unique opportunities for the fabrication over large scales of any complex three-dimensional optical nanodevices, which could also be integrated with silicon processing technologies. Although much development is still required, potential sought-after IR applications would range from low loss photonic waveguides to highly sensitive chemical and imaging detection devices on-chip, able to interact with free-space photons at stand-off distances [262].

Acknowledgments

The authors acknowledge helpful discussions with Dr. John Boeckl from the Materials Directorate, Air Force Research Laboratory, Dayton, OH, and Dr. Dennis Delic, from the Defense Science and Technology group in Edinburgh, SA, Australia. FI and PR gratefully acknowledge the Commonwealth of Australia, represented by the Defense Science and Technology Group, for the project-based funding agreement No.8673. JDC acknowledges support from Office of Naval Research Grant N00014-18-12107, while JGF acknowledges support from Vanderbilt School of Engineering.

ORCID iDs

Patrick Rufangura https://orcid.org/0000-0003-3093-1618 Francesca Iacopi https://orcid.org/0000-0002-3196-0990

References

- [1] Geim A K 2009 Graphene: status and prospects science 324 1530-4
- [2] Novoselov K S, Geim A K, Morozov S V, Jiang D, Zhang Y, Dubonos S V, Grigorieva I V and Firsov A A 2004 Electric field effect in atomically thin carbon films *science* 306 666–9
- [3] Berger C, Song Z, Li T, Li X, Ogbazghi A Y, Feng R, Dai Z, Marchenkov A N, Conrad E H and First P N 2004 Ultrathin epitaxial graphite: 2D electron gas properties and a route toward graphene-based nanoelectronics *J. Phys. Chem.* B 108 19912–6
- [4] Wang R, Ren X-G, Yan Z, Jiang L-J, Wei E and Shan G-C 2019 Graphene based functional devices: A short review Front. Phys. 14 13603
- [5] Xiong L, Forsythe C, Jung M, McLeod A, Sunku S, Shao Y, Ni G, Sternbach A, Liu S and Edgar J 2019 Photonic crystal for graphene plasmons Nat. Commun. 10 1–6
- [6] Caldwell J D, Anderson T J, Culbertson J C, Jernigan G G, Hobart K D, Kub F J, Tadjer M J, Tedesco J L, Hite J K and Mastro M A 2010 Technique for the dry transfer of epitaxial graphene onto arbitrary substrates ACS Nano 4 1108–14
- [7] Cunning B V, Ahmed M, Mishra N, Kermany A R, Wood B and Iacopi F 2014 Graphitized silicon carbide microbeams: wafer-level, self-aligned graphene on silicon wafers *Nanotechnology* 25 325301
- [8] De Heer W A, Berger C, Ruan M, Sprinkle M, Li X, Hu Y, Zhang B, Hankinson J and Conrad E 2011 Large area and structured epitaxial graphene produced by confinement controlled sublimation of silicon carbide *Proc. Natl Acad. Sci.* 108 16900–5
- [9] De Heer W A, Berger C, Wu X, First P N, Conrad E H, Li X, Li T, Sprinkle M, Hass J and Sadowski M L 2007 Epitaxial graphene Solid State Commun. 143 92–100
- [10] Raman A P, Anoma M A, Zhu L, Rephaeli E and Fan S 2014 Passive radiative cooling below ambient air temperature under direct sunlight Nature 515 540
- [11] Rephaeli E, Raman A and Fan S 2013 Ultrabroadband photonic structures to achieve high-performance daytime radiative cooling Nano Lett. 13 1457–61
- [12] Bronzino J D and Diakides N A 2007 Medical Infrared Imaging (Boca Raton, FL: CRC Press)
- [13] Rastinehad A R, Anastos H, Wajswol E, Winoker J S, Sfakianos J P, Doppalapudi S K, Carrick M R, Knauer C J, Taouli B and Lewis S C 2019 Gold nanoshell-localized photothermal ablation of prostate tumors in a clinical pilot device study *Proc. Natl Acad. Sci.* 116 18590–6
- [14] Dall'O G, Sarto L and Panza A 2013 Infrared screening of residential buildings for energy audit purposes: results of a field test Energies 6 3859–78
- [15] Bakker J M, Mac Aleese L, Meijer G and von Helden G 2003 Fingerprint IR spectroscopy to probe amino acid conformations in the gas phase Phys. Rev. Lett. 91 203003
- [16] Keirsse J, Boussard-Pledel C, Loreal O, Sire O, Bureau B, Leroyer P, Turlin B and Lucas J 2003 IR optical fiber sensor for biomedical applications Vib. Spectrosc. 32 23–32
- [17] Adato R and Altug H 2013 In-situ ultra-sensitive infrared absorption spectroscopy of biomolecule interactions in real time with plasmonic nanoantennas Nat. Commun. 4 2154
- [18] Caldwell J D, Glembocki O, Bezares F J, Bassim N D, Rendell R W, Feygelson M, Ukaegbu M, Kasica R, Shirey L and Hosten C 2011 Plasmonic nanopillar arrays for large-area, high-enhancement surface-enhanced Raman scattering sensors ACS Nano 5 4046–55
- [19] Tame M S, McEnery K, Ş Ö, Lee J, Maier S and Kim M 2013 Quantum plasmonics Nat. Phys. 9 329-40
- [20] Welford K 1991 Surface plasmon-polaritons and their uses Opt. Quantum Electron. 23 1-27
- [21] Li P, Lewin M, Kretinin A V, Caldwell J D, Novoselov K S, Taniguchi T, Watanabe K, Gaussmann F and Taubner T 2015 Hyperbolic phonon-polaritons in boron nitride for near-field optical imaging and focusing *Nat. Commun.* 6 7507

- [22] Brar V W, Jang M S, Sherrott M, Kim S, Lopez J J, Kim L B, Choi M and Atwater H 2014 Hybrid surface-phonon-plasmon polariton modes in graphene/monolayer h-BN heterostructures Nano Lett. 14 3876–80
- [23] Foteinopoulou S, Devarapu G C R, Subramania G S, Krishna S and Wasserman D 2019 Phonon-polaritonics: enabling powerful capabilities for infrared photonics *Nanophotonics* 8 2129–75
- [24] Ferrari A C, Bonaccorso F, Fal'Ko V, Novoselov K S, Roche S, Bøggild P, Borini S, Koppens F H, Palermo V and Pugno N 2015 Science and technology roadmap for graphene, related two-dimensional crystals, and hybrid systems Nanoscale 7 4598–810
- [25] Dai S, Ma Q, Liu M, Andersen T, Fei Z, Goldflam M, Wagner M, Watanabe K, Taniguchi T and Thiemens M 2015 Graphene on hexagonal boron nitride as a tunable hyperbolic metamaterial *Nat. Nanotechnol.* 10 682–6
- [26] Dai S, Ma Q, Andersen T, Mcleod A, Fei Z, Liu M, Wagner M, Watanabe K, Taniguchi T and Thiemens M 2015 Subdiffractional focusing and guiding of polaritonic rays in a natural hyperbolic material *Nat. Commun.* 6 1–7
- [27] Caldwell J D, Lindsay L, Giannini V, Vurgaftman I, Reinecke T L, Maier S A and Glembocki O J 2015 Low-loss, infrared and terahertz nanophotonics using surface phonon polaritons Nanophotonics 4 44–68
- [28] Shalaev V M, Cai W, Chettiar U K, Yuan H-K, Sarychev A K, Drachev V P and Kildishev A V 2005 Negative index of refraction in optical metamaterials Opt. Lett. 30 3356–8
- [29] Koppens F H, Chang D E and García de Abajo F J 2011 Graphene plasmonics: a platform for strong light–matter interactions Nano Lett. 11 3370–7
- [30] Jablan M, Soljačić M and Buljan H 2013 Plasmons in graphene: fundamental properties and potential applications Proc. IEEE 101 1689–704
- [31] Luo X, Qiu T, Lu W and Ni Z 2013 Plasmons in graphene: recent progress and applications Mater. Sci. Eng. R 74 351-76
- [32] Razdolski I, Chen Y, Giles A J, Gewinner S, Schöllkopf W, Hong M, Wolf M, Giannini V, Caldwell J D and Maier S A 2016 Resonant enhancement of second-harmonic generation in the mid-infrared using localized surface phonon polaritons in subdiffractional nanostructures Nano Lett. 16 6954–9
- [33] Fei Z, Rodin A, Andreev G O, Bao W, McLeod A, Wagner M, Zhang L, Zhao Z, Thiemens M and Dominguez G 2012 Gate-tuning of graphene plasmons revealed by infrared nano-imaging *Nature* 487 82–5
- [34] Hillenbrand R, Taubner T and Keilmann F 2002 Phonon-enhanced light–matter interaction at the nanometre scale *Nature* 418 159–62
- [35] Tuskan G A, Difazio S, Jansson S, Bohlmann J, Grigoriev I, Hellsten U, Putnam N, Ralph S, Rombauts S and Salamov A 2006 The genome of black cottonwood, Populus trichocarpa (Torr. & Gray) science 313 1596–604
- [36] Mak K F and Shan J 2016 Photonics and optoelectronics of 2D semiconductor transition metal dichalcogenides Nat. Photon. 10 216
- [37] Folland T G and Caldwell J D 2017 Semiconductor Nanophotonics Using Surface Polaritons. In: Advanced Study Institute on NATO ASI on Quantum Nano-Photonics, (ed Baldassare Di Bartolo, et al.: Springer) pp 235–54
- [38] Folland T, Nordin L, Wasserman D and Caldwell J 2019 Probing polaritons in the mid-to far-infrared J. Phys. D: Appl. Phys. 125 191102
- [39] Takahara J, Yamagishi S, Taki H, Morimoto A and Kobayashi T 1997 Guiding of a one-dimensional optical beam with nanometer diameter Opt. Lett. 22 475–7
- [40] Maier S A 2007 Plasmonics: fundamentals and applications (New York, U. S. A: Springer Science & Business Media)
- [41] Low T and Avouris P 2014 Graphene plasmonics for terahertz to mid-infrared applications ACS Nano 8 1086–101
- [42] Low T, Chaves A, Caldwell J D, Kumar A, Nx F, Avouris P, Tf H, Guinea F, Martin-Moreno L and Koppens F 2017 Polaritons in layered two-dimensional materials Nat. Mater. 16 182–94
- [43] Basov D, Fogler M and De Abajo F G 2016 Polaritons in van der Waals materials Science 354 aag1992
- [44] Law S, Podolskiy V and Wasserman D 2013 Towards nano-scale photonics with micro-scale photons: the opportunities and challenges of mid-infrared plasmonics Nanophotonics 2 103–30
- [45] Gramotnev D K and Bozhevolnyi S I 2010 Plasmonics beyond the diffraction limit *Nat. Photon.* 4 83
- [46] Barnes W L, Dereux A and Ebbesen T W 2003 Surface plasmon subwavelength optics nature 424 824
- [47] Zayats A V, Smolyaninov I I and Maradudin A A 2005 Nano-optics of surface plasmon polaritons Phys. Rep. 408 131-314
- [48] Hutter E and Fendler J H 2004 Exploitation of localized surface plasmon resonance Adv. Mater. 16 1685-706
- [49] Zhong Y, Malagari S D, Hamilton T and Wasserman D M 2015 Review of mid-infrared plasmonic materials J. Nanophoton. 9 093791
- [50] Brolo A G 2012 Plasmonics for future biosensors Nat. Photon. 6 709
- [51] Atwater H A and Polman A 2010 Plasmonics for improved photovoltaic devices Nat. Mater. 9 205
- [52] Gangadharan D T, Xu Z, Liu Y, Izquierdo R and Ma D 2017 Recent advancements in plasmon-enhanced promising third-generation solar cells Nanophotonics 6 153–75
- [53] Huang X, Jain P K, El-Sayed I H and El-Sayed M A 2008 Plasmonic photothermal therapy (PPTT) using gold nanoparticles Lasers Med. Sci. 23 217
- [54] Hirsch L R, Stafford R J, Bankson J A, Sershen S R, Rivera B, Price R, Hazle J D, Halas N J and West J L 2003 Nanoshell-mediated near-infrared thermal therapy of tumors under magnetic resonance guidance Proc. Natl Acad. Sci. 100 13549–54
- [55] Zia R, Schuller J A, Chandran A and Brongersma M L 2006 Plasmonics: the next chip-scale technology Mater. Today 9 20–27
- [56] Ju L, Geng B, Horng J, Girit C, Martin M, Hao Z, Bechtel H A, Liang X, Zettl A and Shen Y R 2011 Graphene plasmonics for tunable terahertz metamaterials Nat. Nanotechnol. 6 630
- [57] Yu N and Capasso F 2014 Flat optics with designer metasurfaces *Nat. Mater.* 13 139–50
- [58] Iorsh I V, Mukhin I S, Shadrivov I V, Belov P A and Kivshar Y S 2013 Hyperbolic metamaterials based on multilayer graphene structures Phys. Rev. B 87 075416
- [59] Zheludev N I and Kivshar Y S 2012 From metamaterials to metadevices Nat. Mater. 11 917-24
- [60] Tretyakov S, Urbas A and Zheludev N 2017 Special issue on the history of metamaterials J. Opt. 19 080404
- [61] Engheta N 2007 Circuits with light at nanoscales: optical nanocircuits inspired by metamaterials Science 317 1698-702
- [62] Engheta N and Ziolkowski R W 2006 Metamaterials: Physics and Engineering Explorations (New York: Wiley)
- [63] Barnes W L 2006 Surface plasmon-polariton length scales: a route to sub-wavelength optics J. Opt. A: Pure Appl. Opt. 8 S87
- [64] Atwater H A 2007 The promise of plasmonics Sci. Am. 296 56–62
- [65] Naik G V, Shalaev V M and Boltasseva A 2013 Alternative plasmonic materials: beyond gold and silver Adv. Mater. 25 3264-94
- [66] Murray W A and Barnes W L 2007 Plasmonic materials Adv. Mater. 19 3771-82
- [67] Law S, Adams D, Taylor A and Wasserman D 2012 Mid-infrared designer metals Opt. Express 20 12155-65
- [68] Law S, Liu R and Wasserman D 2014 Doped semiconductors with band-edge plasma frequencies J. Vac. Sci. Technol. B 32 052601

- [69] Boltasseva A and Atwater H A 2011 Low-loss plasmonic metamaterials Science 331 290-1
- [70] Sachet E, Shelton C T, Harris J S, Gaddy B E, Irving D L, Curtarolo S, Donovan B F, Hopkins P E, Sharma P A and Sharma A L 2015 Dysprosium-doped cadmium oxide as a gateway material for mid-infrared plasmonics *Nat. Mater.* 14 414
- [71] Runnerstrom E L, Kelley K P, Folland T G, Nolen J R, Engheta N, Caldwell J D and Maria J-P 2018 Polaritonic hybrid-epsilon-near-zero modes: beating the plasmonic confinement vs propagation-length trade-off with doped cadmium oxide bilayers Nano Lett. 19 948–57
- [72] Nolen J R, Runnerstrom E L, Kelley K P, Luk T S, Folland T G, Cleri A, Maria J-P and Caldwell J D 2020 Ultraviolet to far-infrared dielectric function of n-doped cadmium oxide thin films *Physical Review Materials* 4 025202
- [73] Hsieh W T, Wu P C, Khurgin J B, Tsai D P, Liu N and Sun G 2017 Comparative analysis of metals and alternative infrared plasmonic materials ACS Photon. 5 2541–8
- [74] Khurgin J B 2018 Relative merits of phononics vs. plasmonics: the energy balance approach Nanophotonics 7 305-16
- [75] Economou E 1969 Surface plasmons in thin films Phys. Rev. 182 539
- [76] Burke J, Stegeman G and Tamir T 1986 Surface-polariton-like waves guided by thin, lossy metal films Phys. Rev. B 33 5186
- [77] Zia R, Selker M D, Catrysse P B and Brongersma M L 2004 Geometries and materials for subwavelength surface plasmon modes Josa A 21 2442–6
- [78] Raether H 1988 Surface Plasmons on Smooth and Rough Surfaces and on Gratings (Berlin: Springer) pp 4-39
- [79] Kretschmann E and Raether H 1968 Radiative decay of non radiative surface plasmons excited by light Z Naturforsch. A 23 2135-6
- [80] Otto A 1968 Excitation of nonradiative surface plasma waves in silver by the method of frustrated total reflection *Z. Phys.* A 216 398–410
- [81] Kretschmann E 1972 Decay of non radiative surface plasmons into light on rough silver films. Comparison of experimental and theoretical results *Opt. Commun.* 6 185–7
- [82] Ropers C, Neacsu C, Elsaesser T, Albrecht M, Raschke M and Lienau C 2007 Grating-coupling of surface plasmons onto metallic tips: a nanoconfined light source Nano Lett. 7 2784–8
- [83] Knight M W, Grady N K, Bardhan R, Hao F, Nordlander P and Halas N J 2007 Nanoparticle-mediated coupling of light into a nanowire Nano Lett. 7 2346–50
- [84] Bohren C F and Huffman D R 2008 Absorption and Scattering of Light by Small Particles (New York: Wiley)
- [85] Decker M and Staude I 2016 Resonant dielectric nanostructures: a low-loss platform for functional nanophotonics J. Opt. 18 103001
- [86] Sarid D and Challener W A 2010 Modern Introduction to Surface Plasmons: Theory, Mathematica Modeling, and Applications (Cambridge: Cambridge University Press)
- [87] Li X, Cai W, An J, Kim S, Nah J, Yang D, Piner R, Velamakanni A, Jung I and Tutuc E 2009 Large-area synthesis of high-quality and uniform graphene films on copper foils *science* 324 1312–4
- [88] Reina A, Jia X, Ho J, Nezich D, Son H, Bulovic V, Dresselhaus M S and Kong J 2008 Large area, few-layer graphene films on arbitrary substrates by chemical vapor deposition Nano Lett. 9 30–35
- [89] Chen J-H, Jang C, Adam S, Fuhrer M, Williams E and Ishigami M 2008 Charged-impurity scattering in graphene Nat. Phys. 4 377
- [90] Ovid'Ko I 2013 Mechanical properties of graphene Rev. Adv. Mater. Sci. 34 1–11
- [91] Nair R R, Blake P, Grigorenko A N, Novoselov K S, Booth T J, Stauber T, Peres N M and Geim A K 2008 Fine structure constant defines visual transparency of graphene *Science* 320 1308-
- [92] Lee C, Wei X, Kysar J W and Hone J 2008 Measurement of the elastic properties and intrinsic strength of monolayer graphene science 321 385–8
- [93] Novoselov K S, Geim A K, Morozov S, Jiang D, Katsnelson M, Grigorieva I, Dubonos S and Firsov A A 2005 Two-dimensional gas of massless Dirac fermions in graphene nature 438 197
- [94] Bostwick A, Ohta T, Seyller T, Horn K and Rotenberg E 2007 Quasiparticle dynamics in graphene Nat. Phys. 3 36
- [95] Bolotin K I, Sikes K, Jiang Z, Klima M, Fudenberg G, Hone J, Kim P and Stormer H 2008 Ultrahigh electron mobility in suspended graphene *Solid State Commun.* 146 351–5
- [96] Koppens F H, Chang D E and García de Abajo F J 2011 Graphene plasmonics: a platform for strong light–matter interactions Nano letters 11 3370–7
- [97] Woessner A, Lundeberg M B, Gao Y, Principi A, Alonso-González P, Carrega M, Watanabe K, Taniguchi T, Vignale G and Polini M 2015 Highly confined low-loss plasmons in graphene–boron nitride heterostructures *Nat. Mater.* 14 421–5
- [98] Chen J, Badioli M, Alonso-González P, Thongrattanasiri S, Huth F, Osmond J, Spasenović M, Centeno A, Pesquera A and Godignon P 2012 Optical nano-imaging of gate-tunable graphene plasmons *Nature* 487 77
- [99] Brar V W, Jang M S, Sherrott M, Lopez J J and Atwater H A 2013 Highly confined tunable mid-infrared plasmonics in graphene nanoresonators Nano Lett. 13 2541–7
- [100] Fei Z, Rodin A, Andreev G, Bao W, McLeod A, Wagner M, Zhang L, Zhao Z, Thiemens M and Dominguez G 2012 Gate-tuning of graphene plasmons revealed by infrared nano-imaging *Nature* 487 82
- [101] Zhu W, Rukhlenko I D and Premaratne M 2013 Graphene metamaterial for optical reflection modulation Appl. Phys. Lett. 102 241914
- [102] Rodrigo D, Limaj O, Janner D, Etezadi D, De Abajo F J G, Pruneri V and Altug H 2015 Mid-infrared plasmonic biosensing with graphene Science 349 165–8
- [103] Bonaccorso F, Sun Z, Hasan T and Ferrari A 2010 Graphene photonics and optoelectronics Nat. Photon. 4 611
- [104] Cox J D and De Abajo F J G 2014 Electrically tunable nonlinear plasmonics in graphene nanoislands Nat. Commun. 5 5725
- [105] Grigorenko A, Polini M and Novoselov K 2012 Graphene plasmonics Nat. Photon. 6 749
- [106] Emani N K, Chung T-F, Ni X, Kildishev A V, Chen Y P and Boltasseva A 2012 Electrically tunable damping of plasmonic resonances with graphene Nano Lett. 12 5202–6
- [107] Fang Z, Thongrattanasiri S, Schlather A, Liu Z, Ma L, Wang Y, Ajayan P M, Nordlander P, Halas N J and García de Abajo F J 2013 Gated tunability and hybridization of localized plasmons in nanostructured graphene ACS Nano 7 2388–95
- [108] Bao Q, Zhang H, Wang B, Ni Z, Lim C H Y X, Wang Y, Tang D Y and Loh K P 2011 Broadband graphene polarizer *Nat. Photon.* 5 411
- [109] Jablan M, Buljan H and Soljačić M 2009 Plasmonics in graphene at infrared frequencies Phys. Rev. B 80 245435
- [110] Huang S, Song C, Zhang G and Yan H 2016 Graphene plasmonics: physics and potential applications Nanophotonics 6 1191–204
- [111] Neto A C, Guinea F, Peres N M, Novoselov K S and Geim A K 2009 The electronic properties of graphene Rev. Mod. Phys. 81 109
- [112] Chen X, Jia B, Zhang Y and Gu M 2013 Exceeding the limit of plasmonic light trapping in textured screen-printed solar cells using Al nanoparticles and wrinkle-like graphene sheets *Light: Sci. Appl.* 2 e92

- [113] Miao X, Tongay S, Petterson M K, Berke K, Rinzler A G, Appleton B R and Hebard A F 2012 High efficiency graphene solar cells by chemical doping *Nano Lett.* 12 2745–50
- [114] Echtermeyer T, Britnell L, Jasnos P, Lombardo A, Gorbachev R, Grigorenko A, Geim A, Ferrari A C and Novoselov K 2011 Strong plasmonic enhancement of photovoltage in graphene *Nat. Commun.* 2 1–5
- [115] Liu Y, Dong X and Chen P 2012 Biological and chemical sensors based on graphene materials Chem. Soc. Rev. 41 2283-307
- [116] Wu L, Chu H, Koh W and Li E 2010 Highly sensitive graphene biosensors based on surface plasmon resonance *Opt. Express* 18 14395–400
- [117] Xia F, Mueller T, Lin Y-M, Valdes-Garcia A and Avouris P 2009 Ultrafast graphene photodetector Nat. Nanotechnol. 4 839
- [118] Gan X, Shiue R-J, Gao Y, Meric I, Heinz T F, Shepard K, Hone J, Assefa S and Englund D 2013 Chip-integrated ultrafast graphene photodetector with high responsivity *Nat. Photon.* 7 883
- [119] Furchi M, Urich A, Pospischil A, Lilley G, Unterrainer K, Detz H, Klang P, Andrews A M, Schrenk W and Strasser G 2012 Microcavity-integrated graphene photodetector Nano Lett. 12 2773–7
- [120] Zhang Y, Liu T, Meng B, Li X, Liang G, Hu X and Wang Q J 2013 Broadband high photoresponse from pure monolayer graphene photodetector *Nat. Commun.* 4 1811
- [121] Mueller T, Xia F and Avouris P 2010 Graphene photodetectors for high-speed optical communications Nat. Photon. 4 297
- [122] Sun Z, Hasan T, Torrisi F, Popa D, Privitera G, Wang F, Bonaccorso F, Basko D M and Ferrari A C 2010 Graphene mode-locked ultrafast laser ACS Nano 4 803–10
- [123] Bao Q, Zhang H, Wang Y, Ni Z, Yan Y, Shen Z X, Loh K P and Tang D Y 2009 Atomic-layer graphene as a saturable absorber for ultrafast pulsed lasers *Adv. Funct. Mater.* 19 3077–83
- [124] Bae S, Kim H, Lee Y, Xu X, Park J-S, Zheng Y, Balakrishnan J, Lei T, Kim H R and Song Y I 2010 Roll-to-roll production of 30-inch graphene films for transparent electrodes *Nat. Nanotechnol.* 5 574
- [125] Rümmeli M H, Gorantla S, Bachmatiuk A, Phieler J, Geissler N, Ibrahim I, Pang J and Eckert J R 2013 On the role of vapor trapping for chemical vapor deposition (CVD) grown graphene over copper Chem. Mater. 25 4861–6
- [126] Rummeli M H, Bachmatiuk A, Scott A, Borrnert F, Warner J H, Hoffman V, Lin J-H, Cuniberti G and Buchner B 2010 Direct low-temperature nanographene CVD synthesis over a dielectric insulator ACS Nano 4 4206–10
- [127] Jiao L, Zhang L, Wang X, Diankov G and Dai H 2009 Narrow graphene nanoribbons from carbon nanotubes Nature 458 877
- [128] Choucair M, Thordarson P and Stride J A 2009 Gram-scale production of graphene based on solvothermal synthesis and sonication *Nat. Nanotechnol.* 4 30
- [129] Emtsev K V, Bostwick A, Horn K, Jobst J, Kellogg G L, Ley L, McChesney J L, Ohta T, Reshanov S A and Röhrl J 2009 Towards wafer-size graphene layers by atmospheric pressure graphitization of silicon carbide Nat. Mater. 8 203–7
- [130] Gupta B, Notarianni M, Mishra N, Shafiei M, Iacopi F and Motta N 2014 Evolution of epitaxial graphene layers on 3C SiC/Si (1: 1 1) as a function of annealing temperature in UHV Carbon 68 563–72
- [131] Seyller T, Bostwick A, Emtsev K, Horn K, Ley L, McChesney J, Ohta T, Riley J D, Rotenberg E and Speck F 2008 Epitaxial graphene: a new material *Phys. Status Solidi* b 245 1436–46
- [132] Mishra N, Boeckl J, Motta N and Iacopi F 2016 Graphene growth on silicon carbide: A review Phys. Status Solidi a 213 2277-89
- [133] Ouerghi A, Marangolo M, Belkhou R, El Moussaoui S, Silly M, Eddrief M, Largeau L, Portail M, Fain B and Sirotti F 2010 Epitaxial graphene on 3C-SiC (111) pseudosubstrate: structural and electronic properties *Phys. Rev.* B **82** 125445
- [134] Miyamoto Y, Handa H, Saito E, Konno A, Narita Y, Suemitsu M, Fukidome H, Ito T, Yasui K and Nakazawa H 2009 Raman-scattering spectroscopy of epitaxial graphene formed on SiC film on Si substrate e-J. Surf. Sci. Nanotechnol. 7 107–9
- [135] Ouerghi A, Kahouli A, Lucot D, Portail M, Travers L, Gierak J, Penuelas J, Jegou P, Shukla A and Chassagne T 2010 Epitaxial graphene on cubic SiC (111)/Si (111) substrate Appl. Phys. Lett. 96 191910
- [136] Gupta B, Placidi E, Hogan C, Mishra N, Iacopi F and Motta N 2015 The transition from 3C SiC (1: 1 1) to graphene captured by ultra high vacuum scanning tunneling microscopy *Carbon* 91 378–85
- [137] Juang Z-Y, Wu C-Y, Lo C-W, Chen W-Y, Huang C-F, Hwang J-C, Chen F-R, Leou K-C and Tsai C-H 2009 Synthesis of graphene on silicon carbide substrates at low temperature *Carbon* 47 2026–31
- [138] Delamoreanu A, Rabot C, Vallee C and Zenasni A 2014 Wafer scale catalytic growth of graphene on nickel by solid carbon source Carbon 66 48–56
- [139] Iacopi F, Mishra N, Bv C, Goding D, Dimitrijev S, Brock R, Dauskardt R H, Wood B and Boeckl J 2015 A catalytic alloy approach for graphene on epitaxial SiC on silicon wafers *J. Mater. Res.* 30 609–16
- [140] Mishra N, Boeckl J J, Tadich A, Jones R T, Pigram P J, Edmonds M, Fuhrer M S, Nichols B M and Iacopi F 2017 Solid source growth of graphene with Ni–Cu catalysts: towards high quality in situ graphene on silicon *J. Phys. D: Appl. Phys.* 50 095302
- [141] Shtepliuk I, Khranovskyy V and Yakimova R 2016 Combining graphene with silicon carbide: synthesis and properties—a review Semicond. Sci. Technol. 31 113004
- [142] Mak K F, Sfeir M Y, Wu Y, Lui C H, Misewich J A and Heinz T F 2008 Measurement of the optical conductivity of graphene Phys. Rev. Lett. 101 196405
- [143] Ziegler K 2007 Minimal conductivity of graphene: nonuniversal values from the Kubo formula Phys. Rev. B 75 233407
- [144] Alaee R, Farhat M, Rockstuhl C and Lederer F 2012 A perfect absorber made of a graphene micro-ribbon metamaterial Opt. Express 20 28017–24
- [145] Hanson G W 2008 Quasi-transverse electromagnetic modes supported by a graphene parallel-plate waveguide J. Phys. D: Appl. Phys. 104 084314
- [146] Vakil A and Engheta N 2011 Transformation optics using graphene Science 332 1291-4
- [147] Wang B, Zhang X, García-Vidal F J, Yuan X and Teng J 2012 Strong coupling of surface plasmon polaritons in monolayer graphene sheet arrays Phys. Rev. Lett. 109 073901
- [148] Runnerstrom E L, Kelley K P, Sachet E, Shelton C T and Maria J-P 2017 Epsilon-near-zero modes and surface plasmon resonance in fluorine-doped cadmium oxide thin films ACS Photon. 4 1885–92
- [149] Campione S, Brener I and Marquier F 2015 Theory of epsilon-near-zero modes in ultrathin films Phys. Rev. B 91 121408
- [150] Vassant S, Hugonin J-P, Marquier F and Greffet -J-J 2012 Berreman mode and epsilon near zero mode Opt. Express 20 23971-7
- [151] Dastmalchi B, Tassin P, Koschny T and Soukoulis C M 2016 A new perspective on plasmonics: confinement and propagation length of surface plasmons for different materials and geometries *Adv. Opt. Mater.* 4 177–84
- [152] Garcia de Abajo F J 2014 Graphene plasmonics: challenges and opportunities Acs Photon. 1 135-52
- [153] Guo Q, Li C, Deng B, Yuan S, Guinea F and Xia F 2017 Infrared nanophotonics based on graphene plasmonics *ACS Photon*. 4 2989–99

- [154] Fan Y, Liu Z, Zhang F, Zhao Q, Wei Z, Fu Q, Li J, Gu C and Li H 2015 Tunable mid-infrared coherent perfect absorption in a graphene meta-surface Sci. Rep. 5 13956
- [155] Torres L E F, Roche S and Charlier J-C 2020 Introduction to Graphene-based Nanomaterials: From Electronic Structure to Quantum Transport (Cambridge: Cambridge University Press)
- [156] Guo Q, Yu R, Li C, Yuan S, Deng B, Fjg D A and Xia F 2018 Efficient electrical detection of mid-infrared graphene plasmons at room temperature *Nat. Mater.* 17 986–92
- [157] Shiue R-J, Gao Y, Tan C, Peng C, Zheng J, Efetov D K, Kim Y D, Hone J and Englund D 2019 Thermal radiation control from hot graphene electrons coupled to a photonic crystal nanocavity *Nat. Commun.* 10 1–7
- [158] Chakraborty S, Marshall O, Folland T, Kim Y-J, Grigorenko A and Novoselov K 2016 Gain modulation by graphene plasmons in aperiodic lattice lasers *Science* 351 246–8
- [159] Lundeberg M B, Gao Y, Asgari R, Tan C, Van Duppen B, Autore M, Alonso-González P, Woessner A, Watanabe K and Taniguchi T 2017 Tuning quantum nonlocal effects in graphene plasmonics Science 357 187–91
- [160] Ni G, McLeod A, Sun Z, Wang L, Xiong L, Post K, Sunku S, Jiang B-Y, Hone J and Dean C R 2018 Fundamental limits to graphene plasmonics *Nature* 557 530–3
- [161] Yu L, Zheng J, Xu Y, Dai D and He S 2014 Local and nonlocal optically induced transparency effects in graphene–silicon hybrid nanophotonic integrated circuits ACS Nano 8 11386–93
- [162] Silveiro I, Ortega J M P and De Abajo F J G 2015 Quantum nonlocal effects in individual and interacting graphene nanoribbons Light: Sci. Appl. 4 e241-e
- [163] Sunku S, Ni G, Jiang B-Y, Yoo H, Sternbach A, McLeod A, Stauber T, Xiong L, Taniguchi T and Watanabe K 2018 Photonic crystals for nano-light in moiré graphene superlattices Science 362 1153–6
- [164] Ryzhii V and Ryzhii M 2009 Graphene bilayer field-effect phototransistor for terahertz and infrared detection Phys. Rev. B 79 245311
- [165] Ju L, Wang L, Cao T, Taniguchi T, Watanabe K, Louie S G, Rana F, Park J, Hone J and Wang F 2017 Tunable excitons in bilayer graphene Science 358 907–10
- [166] Bolotin K I, Sikes K J, Jiang Z, Klima M, Fudenberg G, Hone J, Kim P and Stormer H 2008 Ultrahigh electron mobility in suspended graphene Solid state communications 146 351–5
- [167] Pradeepkumar A, Amjadipour M, Mishra N, Liu C, Fuhrer M S, Bendavid A, Isa F, Zielinski M, Sirikumara H I, Jayasekara T, Gaskill D K and Iacopi F 2019 p-Type Epitaxial Graphene on Cubic Silicon Carbide on Silicon for Integrated Silicon Technologies ACS Applied Nano Materials 3 830–41
- [168] Efetov D K and Kim P 2010 Controlling electron-phonon interactions in graphene at ultrahigh carrier densities Phys. Rev. Lett. 105 256805
- [169] Yao Y, Shankar R, Kats M A, Song Y, Kong J, Loncar M and Capasso F 2014 Electrically tunable metasurface perfect absorbers for ultrathin mid-infrared optical modulators *Nano Lett.* 14 6526–32
- [170] Li Z and Yu N 2013 Modulation of mid-infrared light using graphene-metal plasmonic antennas Appl. Phys. Lett. 102 131108
- [171] Emani N K, Chung T-F, Kildishev A V, Shalaev V M, Chen Y P and Boltasseva A 2013 Electrical modulation of fano resonance in plasmonic nanostructures using graphene *Nano Lett.* 14 78–82
- [172] Sensale-Rodriguez B, Yan R, Kelly M M, Fang T, Tahy K, Hwang W S, Jena D, Liu L and Xing H G 2012 Broadband graphene terahertz modulators enabled by intraband transitions Nat. Commun. 3 1–7
- [173] Lee S H, Choi M, Kim -T-T, Lee S, Liu M, Yin X, Choi H K, Lee S S, Choi C-G and Choi S-Y 2012 Switching terahertz waves with gate-controlled active graphene metamaterials *Nat. Mater.* 11 936–41
- [174] Zhang Q, Zhen Z, Yang Y, Gan G, Jariwala D and Cui X 2019 Hybrid phonon-polaritons at atomically-thin van der Waals heterointerfaces for infrared optical modulation *Opt. Express* 27 18585–600
- [175] Kim J T, Yu Y-J, Choi H and Choi C-G 2014 Graphene-based plasmonic photodetector for photonic integrated circuits Opt. Express 22 803–8
- [176] Wang X, Cheng Z, Xu K, Tsang H K and Xu J-B 2013 High-responsivity graphene/silicon-heterostructure waveguide photodetectors Nat. Photon. 7 888
- [177] Yang K, Liu S, Arezoomandan S, Nahata A and Sensale-Rodriguez B 2014 Graphene-based tunable metamaterial terahertz filters Appl. Phys. Lett. 105 093105
- [178] Li H-J, Wang -L-L, Zhang H, Huang Z-R, Sun B, Zhai X and Wen S-C 2014 Graphene-based mid-infrared, tunable, electrically controlled plasmonic filter Appl. Phys. Express 7 024301
- [179] Moon J, Curtis D, Bui S, Hu M, Gaskill D, Tedesco J, Asbeck P, Jernigan G, VanMil B and Myers-Ward R 2010 Top-gated epitaxial graphene FETs on Si-face SiC wafers with a peak transconductance of 600 mS/mm IEEE Electron Device Lett. 31 260–2
- [180] Kedzierski J, Hsu P-L, Healey P, Wyatt P W, Keast C L, Sprinkle M, Berger C and De Heer W A 2008 Epitaxial graphene transistors on SiC substrates *IEEE Trans. Electron Devices* 55 2078–85
- [181] Oostinga J B, Heersche H B, Liu X, Morpurgo A F and Vandersypen L M 2008 Gate-induced insulating state in bilayer graphene devices Nat. Mater. 7 151
- [182] Jung N, Kim N, Jockusch S, Turro N J, Kim P and Brus L 2009 Charge transfer chemical doping of few layer graphenes: charge distribution and band gap formation *Nano Lett.* 9 4133–7
- [183] Yu Y-J, Zhao Y, Ryu S, Brus L E, Kim K S and Kim P 2009 Tuning the graphene work function by electric field effect *Nano Lett.* 9 3430–4
- [184] Fanton M, Robinson J, Weiland B and Moon J 2019 3C-SiC Films Grown on Si(111) Substrates as a Template for Graphene Epitaxy ECS Transactions 19 131–5
- [185] Pirouz P, Chorey C and Powell J 1987 Antiphase boundaries in epitaxially grown β-SiC Appl. Phys. Lett. 50 221–3
- [186] Song X, Michaud J, Cayrel F, Zielinski M, Portail M, Chassagne T, Collard E and Alquier D 2010 Microtwin reduction in 3C–SiC heteroepitaxy Appl. Phys. Lett. 96 142104
- [187] Pradeepkumar A, Zielinski M, Bosi M, Verzellesi G, Gaskill D K and Iacopi F 2018 Electrical leakage phenomenon in heteroepitaxial cubic silicon carbide on silicon *J. Phys. D: Appl. Phys.* 123 215103
- [188] Hu H, Zhai F, Hu D, Li Z, Bai B, Yang X and Dai Q 2015 Broadly tunable graphene plasmons using an ion-gel top gate with low control voltage *Nanoscale* 7 19493–500
- [189] Yan H, Li Z, Li X, Zhu W, Avouris P and Xia F 2012 Infrared spectroscopy of tunable Dirac terahertz magneto-plasmons in graphene *Nano Lett.* 12 3766–71
- [190] Kumar A, Low T, Fung K H, Avouris P and Fang N X 2015 Tunable light–matter interaction and the role of hyperbolicity in graphene–hBN system *Nano Lett.* 15 3172–80

- [191] Yan H, Li X, Chandra B, Tulevski G, Wu Y, Freitag M, Zhu W, Avouris P and Xia F 2012 Tunable infrared plasmonic devices using graphene/insulator stacks Nat. Nanotechnol. 7 330–4
- [192] Fang Z, Wang Y, Schlather A E, Liu Z, Ajayan P M, Fj G D A, Nordlander P, Zhu X and Halas N J 2014 Active tunable absorption enhancement with graphene nanodisk arrays *Nano Lett.* 14 299–304
- [193] Koch R, Fryska S, Ostler M, Endlich M, Speck F, Hänsel T, Schaefer J and Seyller T 2016 Robust phonon-plasmon coupling in quasifreestanding graphene on silicon carbide *Phys. Rev. Lett.* **116** 106802
- [194] Koch R, Seyller T and Schaefer J 2010 Strong phonon-plasmon coupled modes in the graphene/silicon carbide heterosystem *Phys. Rev.* B 82 201413
- [195] Xiao X, Li X, Caldwell J D, Maier S A and Giannini V 2018 Theoretical analysis of graphene plasmon cavities Appl. Mater. Today 12 283–93
- [196] Adachi S 2012 Optical properties of crystalline and amorphous semiconductors: Materials and fundamental principles (New York, U. S. A: Springer Science & Business Media)
- [197] Caldwell J D, Glembocki O J, Francescato Y, Sharac N, Giannini V, Bezares F J, Long J P, Owrutsky J C, Vurgaftman I and Tischler J G 2013 Low-loss, extreme subdiffraction photon confinement via silicon carbide localized surface phonon polariton resonators Nano Lett. 13 3690–7
- [198] Luxmoore I J, Gan C H, Liu P Q, Valmorra F, Li P, Faist J R M and Nash G R 2014 Strong coupling in the far-infrared between graphene plasmons and the surface optical phonons of silicon dioxide ACS Photon. 1 1151–5
- [199] Mooradian A and Wright G 1966 Observation of the interaction of plasmons with longitudinal optical phonons in GaAs Phys. Rev. Lett. 16 999
- [200] García Núñez C, Braña A F, Pau J L, Ghita D, García B J, Shen G, Wilbert D, Kim S and Kung P 2014 Surface optical phonons in GaAs nanowires grown by Ga-assisted chemical beam epitaxy J. Phys. D: Appl. Phys. 115 034307
- [201] Nienhaus H, Kampen T and Mönch W 1995 Phonons in 3C-, 4H-, and 6H-SiC Surf. Sci. 324 L328-L32
- [202] Dai S, Fang W, Rivera N, Stehle Y, Jiang B Y, Shen J, Tay R Y, Ciccarino C J, Ma Q and Rodan-Legrain D 2019 Phonon polaritons in monolayers of hexagonal boron nitride *Adv. Mater.* 31 1806603
- [203] Fali A, White S T, Folland T G, He M, Aghamiri N A, Liu S, Edgar J H, Caldwell J D, Haglund R F and Abate Y 2019 Refractive index-based control of hyperbolic phonon-polariton propagation Nano Lett. 19 7725–34
- [204] Chatzakis I, Krishna A, Culbertson J, Sharac N, Giles A J, Spencer M G and Caldwell J D 2018 Strong confinement of optical fields using localized surface phonon polaritons in cubic boron nitride Opt. Lett. 43 2177–80
- [205] Caldwell J D, Kretinin A V, Chen Y, Giannini V, Fogler M M, Francescato Y, Ellis C T, Tischler J G, Woods C R and Giles A J 2014 Sub-diffractional volume-confined polaritons in the natural hyperbolic material hexagonal boron nitride Nat. Commun. 5 5221
- [206] Tamagnone M, Ambrosio A, Chaudhary K, Jauregui L A, Kim P, Wilson W L and Capasso F 2018 Ultra-confined mid-infrared resonant phonon polaritons in van der Waals nanostructures Sci. Adv. 4 eaat7189
- [207] Lee I-H, He M, Zhang X, Luo Y, Liu S, Edgar J H, Wang K, Avouris P, Low T and Caldwell J D 2020 Pushing the polariton confinement limits with low losses using image polaritons in boron nitride *arXiv:2001.10583*
- [208] Feng K, Streyer W, Zhong Y, Hoffman A and Wasserman D 2015 Photonic materials, structures and devices for Reststrahlen optics Opt. Express 23 A1418–A33
- [209] Patrick L and Choyke W 1973 Localized vibrational modes of a persistent defect in ion-implanted SiC J. Phys. Chem. Solids 34 565–7
- [210] Gubbin C R, Martini F, Politi A, Maier S A and De Liberato S 2016 Strong and coherent coupling between localized and propagating phonon polaritons Phys. Rev. Lett. 116 246402
- [211] Chen Y, Francescato Y, Caldwell J D, Giannini V, Maß T W, Glembocki O J, Bezares F J, Taubner T, Kasica R and Hong M 2014 Spectral tuning of localized surface phonon polariton resonators for low-loss mid-IR applications *Acs Photon.* 1 718–24
- [212] Huber A, Ocelic N, Taubner T and Hillenbrand R 2006 Nanoscale resolved infrared probing of crystal structure and of plasmon— phonon coupling Nano Lett. 6 774–8
- [213] Taubner T, Korobkin D, Urzhumov Y, Shvets G and Hillenbrand R 2006 Near-field microscopy through a SiC superlens *Science* 313 1595-
- [214] Schuller J A, Zia R, Taubner T and Brongersma M L 2007 Dielectric metamaterials based on electric and magnetic resonances of silicon carbide particles *Phys. Rev. Lett.* 99 107401
- [215] Radulaski M, Babinec T M, Müller K, Lagoudakis K G, Zhang J L, Buckley S, Kelaita Y A, Alassaad K, Ferro G and Vucković J 2014 Visible photoluminescence from cubic (3C) silicon carbide microdisks coupled to high quality whispering gallery modes ACS Photon. 2 14–19
- [216] Khramtsov I A, Vyshnevyy A A and Fedyanin D Y 2018 Enhancing the brightness of electrically driven single-photon sources using color centers in silicon carbide *npj Quantum Information* 4 1–8
- [217] Passler N C, Gubbin C R, Folland T G, Razdolski I, Katzer D S, Storm D F, Wolf M, De Liberato S, Caldwell J D and Paarmann A 2018 Strong coupling of epsilon-near-zero phonon polaritons in polar dielectric heterostructures *Nano Lett.* 18 4285–92
- [218] Pufahl K, Passler N C, Grosse N B, Wolf M, Woggon U and Paarmann A 2018 Controlling nanoscale air-gaps for critically coupled surface polaritons by means of non-invasive white-light interferometry Appl. Phys. Lett. 113 161103
- [219] Passler N C, Razdolski I, Gewinner S, Schöllkopf W, Wolf M and Paarmann A 2017 Second-harmonic generation from critically coupled surface phonon polaritons ACS Photon. 4 1048–53
- [220] Gubbin C R, Berte R, Meeker M A, Giles A J, Ellis C T, Tischler J G, Wheeler V D, Maier S A, Caldwell J D and De Liberato S 2019 Hybrid longitudinal-transverse phonon polaritons *Nature communications* 10 1–6
- [221] Gubbin C R, Maier S A and De Liberato S 2017 Theoretical investigation of phonon polaritons in SiC micropillar resonators *Phys. Rev.* B **95** 035313
- [222] Feldman D, Parker J H Jr, Choyke W and Patrick L 1968 Raman scattering in 6 H SiC Phys. Rev. 170 698
- [223] Feldman D, Parker J H Jr, Choyke W and Patrick L 1968 Phonon dispersion curves by raman scattering in SiC, polytypes 3 C, 4 H, 6 H, 1: 5 R, and 2: 1 R *Phys. Rev.* 173 787
- [224] Harima H, Nakashima S I and Uemura T 1995 Raman scattering from anisotropic LO-phonon–plasmon–coupled mode in n-type 4H–and 6H–SiC J. Phys. D: Appl. Phys. 78 1996–2005
- [225] Tiwald T E, Woollam J A, Zollner S, Christiansen J, Gregory R, Wetteroth T, Wilson S and Powell A R 1999 Carrier concentration and lattice absorption in bulk and epitaxial silicon carbide determined using infrared ellipsometry Phys. Rev. B 60 11464
- [226] Hillenbrand R, Taubner T and Keilmann F 2002 Phonon-enhanced light–matter interaction at the nanometre scale *Nature* 418 159–62

- [227] Greffet -J-J, Carminati R, Joulain K, Mulet J-P, Mainguy S and Chen Y 2002 Coherent emission of light by thermal sources *Nature* 416 61–64
- [228] Neuner I I I B, Korobkin D, Fietz C, Carole D, Ferro G and Shvets G 2009 Critically coupled surface phonon-polariton excitation in silicon carbide Opt. Lett. 34 2667–9
- [229] Neuner I I I B, Korobkin D, Fietz C, Carole D, Ferro G and Shvets G 2010 Midinfrared index sensing of pL-scale analytes based on surface phonon polaritons in silicon carbide *J. Phys. Chem.* C 114 7489–91
- [230] Schuller J A, Taubner T and Brongersma M L 2009 Optical antenna thermal emitters Nat. Photon. 3 658
- [231] Wang T, Li P, Hauer B, Chigrin D N and Taubner T 2013 Optical properties of single infrared resonant circular microcavities for surface phonon polaritons *Nano Lett.* 13 5051–5
- [232] Chen Y, Francescato Y, Caldwell J D, Giannini V, Maß T W, Glembocki O J, Bezares F J, Taubner T, Kasica R and Hong M 2014 Spectral tuning of localized surface phonon polariton resonators for low-loss mid-IR applications *Acs Photonics* 1 718–24
- [233] Caldwell J D, Kretinin A V, Chen Y, Giannini V, Fogler M M, Francescato Y, Ellis C T, Tischler J G, Woods C R and Giles A J 2014 Sub-diffractional volume-confined polaritons in the natural hyperbolic material hexagonal boron nitride *Nature communications* 5 1–9
- [234] Lidzey D G, Bradley D, Skolnick M, Virgili T, Walker S and Whittaker D 1998 Strong exciton–photon coupling in an organic semiconductor microcavity Nature 395 53
- [235] Gubbin C R, Berte R, Meeker M A, Giles A J, Ellis C T, Tischler J G, Wheeler V D, Maier S A, Caldwell J D and De Liberato S 2019 Hybrid longitudinal-transverse phonon polaritons *Nat. Commun.* 10 1682
- [236] Folland T G, Lu G, Bruncz A, Nolen J R, Tadjer M and Caldwell J D 2020 Vibrational coupling to epsilon-near-zero waveguide modes ACS Photon. 7 614–21
- [237] Dunkelberger A D et al 2017 Active tuning of surface phonon polariton resonances via carrier photoinjection Nat. Photon. 12 50–56
- [238] Caldwell J D, Vurgaftman I, Tischler J G, Glembocki O J, Owrutsky J C and Reinecke T L 2016 Atomic-scale photonic hybrids for mid-infrared and terahertz nanophotonics Nat. Nanotechnol. 11 9
- [239] Ratchford D C, Winta C J, Chatzakis I, Ellis C T, Passler N C, Winterstein J, Dev P, Razdolski I, Matson J R and Nolen J R 2019 Controlling the infrared dielectric function through atomic-scale heterostructures ACS nano 13 6730–41
- [240] Fei Z, Andreev G O, Bao W, Zhang L M, McLeod A S, Wang C, Stewart M K, Zhao Z, Dominguez G and Thiemens M 2011 Infrared nanoscopy of dirac plasmons at the graphene–SiO₂ interface *Nano Lett.* 11 4701–5
- [241] Santos C N, Joucken F, Meneses D D S, Echegut P, Campos-Delgado J, Louette P, Raskin J-P and Hackens B 2016 Terahertz and mid-infrared reflectance of epitaxial graphene Sci. Rep. 6 24301
- [242] Hwang E, Sensarma R and Sarma S D 2010 Plasmon-phonon coupling in graphene Phys. Rev. B 82 195406
- [243] Liu Y and Willis R F 2010 Plasmon-phonon strongly coupled mode in epitaxial graphene Phys. Rev. B 81 081406
- [244] Dai S, Ma Q, Liu M, Andersen T, Fei Z, Goldflam M, Wagner M, Watanabe K, Taniguchi T and Thiemens M 2015 Graphene on hexagonal boron nitride as a tunable hyperbolic metamaterial *Nature nanotechnology* 10 682–6
- [245] Radulaski M, Babinec T M, Buckley S, Rundquist A, Provine J, Alassaad K, Ferro G and Vučković J 2013 Photonic crystal cavities in cubic (3C) polytype silicon carbide films *Opt. Express* 21 32623–9
- [246] Song B-S, Yamada S, Asano T and Noda S 2011 Demonstration of two-dimensional photonic crystals based on silicon carbide Opt. Express 19 11084–9
- [247] Geim A K and Novoselov K S 2007 The rise of graphene Nat. Mater. 6 183
- [248] Matz R and Lüth H 1981 Conduction-band surface plasmons in the electron-energy-loss spectrum of GaAs (110) Phys. Rev. Lett. 46 500
- [249] Matz R and Lüth H. 1981 Conduction-band surface plasmons in the electron-energy-loss spectrum of GaAs (110) Physical Review Letters 46 500
- [250] Li K, Fitzgerald J M, Xiao X, Caldwell J D, Zhang C, Maier S A, Li X and Giannini V 2017 Graphene plasmon cavities made with silicon carbide ACS Omega 2 3640–6
- [251] Zimmerman W B 2006 Multiphysics Modeling with Finite Element Methods Vol 18 (Singapore: World Scientific Publishing Company)
- [252] Daas B K and Dutta A 2014 Electromagnetic dispersion of surface plasmon polariton at the EG/SiC interface *J. Mater. Res.* **29** 2485–90
- [253] Wang J, Yang L, Wang M, Hu Z-D, Deng Q, Nie Y, Zhang F and Sang T 2018 Perfect absorption and strong magnetic polaritons coupling of graphene-based silicon carbide grating cavity structures J. Phys. D: Appl. Phys. 52 015101
- [254] Langer T, Pfnür H, Tegenkamp C, Forti S, Emtsev K and Starke U 2012 Manipulation of plasmon electron–hole coupling in quasi-free-standing epitaxial graphene layers New J. Phys. 14 103045
- [255] Lu W B, Zhu W, Xu H J, Ni Z H, Dong Z G and Cui T J 2013 Flexible transformation plasmonics using graphene *Opt. Express* 21 10475–82
- [256] Xiao S, Zhu X, Li B-H and Mortensen N A 2016 Graphene-plasmon polaritons: from fundamental properties to potential applications Front. Phys. 11 117801
- [257] Wang Y, Liu H, Wang S, Cai M and Ma L 2019 Optical transport properties of graphene surface plasmon polaritons in mid-infrared band Crystals 9 354
- [258] Khurgin J B 2015 How to deal with the loss in plasmonics and metamaterials Nat. Nanotechnol. 10 2
- [259] Avouris P and Dimitrakopoulos C 2012 Graphene: synthesis and applications Mater. Today 15 86–97
- [260] Whitener K E Jr and Sheehan P E 2014 Graphene synthesis Diam. Relat. Mater. 46 25–34
- [261] Berger C, Song Z, Li X, Wu X, Brown N, Naud C, Mayou D, Li T, Hass J and Marchenkov A N 2006 Electronic confinement and coherence in patterned epitaxial graphene *Science* 312 1191–6
- [262] Yan H, Low T, Zhu W, Wu Y, Freitag M, Li X, Guinea F, Avouris P and Xia F 2013 Damping pathways of mid-infrared plasmons in graphene nanostructures *Nat. Photon.* 7 394